EVALUATION OF MECHANICAL PROPERTIES OF AL-CU COLD SPRAYED AND ALLOY 625 WIRE ARC SPRAYED COATINGS

A Thesis
Submitted to the Graduate Faculty
of the
North Dakota State University
of Agriculture and Applied Science

By

Milad Bashirzadeh

In Partial Fulfillment of the Requirements
for the Degree of
MASTER OF SCIENCE

Major Department:
Mechanical Engineering

August 2013

Fargo, North Dakota

North Dakota State University
Graduate School

Title

Investigation on Mechanical Properties of Al-Cu Cold Sprayed and Alloy 625 Wire Arc Sprayed Coatings

By

Milad Bashirzadeh

The Supervisory Committee certifies that this ***disquisition*** complies with North Dakota State University's regulations and meets the accepted standards for the degree of

MASTER OF SCIENCE

SUPERVISORY COMMITTEE:

Dr. Fardad Azarmi
Chair

Dr. Ghodrat Karami

Dr. Annie Tangpong

Dr. Andrew Croll

Approved:

1/13/2014
Date

Dr. Alan Kallmeyer
Department Chair

ABSTRACT

This study examines microstructural-based mechanical properties of Al-Cu composite deposited by cold spraying and wire arc sprayed nickel-based Alloy 625 coating using numerical modeling and experimental techniques. The microhardness and elastic modulus of samples were determined using the Knoop hardness technique. Hardness in both transverse and longitudinal directions on the sample cross-sections has been measured. An image-based finite element simulation algorithm was employed to determine the mechanical properties through an inverse analysis. In addition mechanical tests including, tensile, bending, and nano-indentation tests were performed on Alloy 625 wire arc sprayed samples. Overall, results from the experimental tests are in relatively good agreement for deposited Al-Cu composites and Alloy 625 coating. However, results obtained from numerical simulation are significantly higher in value than experimentally obtained results. Examination and comparison of the results are strong indications of the influence of microstructure characteristics on the mechanical properties of thermally spray deposited coatings.

ACKNOWLEDGEMENTS

I thank my advisor, Dr. Azarmi, because without his guidance it would have been not possible. I appreciate the support and comments he had for me throughout the study.

I also want to thank Dr. Karami for his assistance with the FEA.

I also want to thank Dr. Tangpong and Dr. Croll for their suggestions and questions that assisted me in preparing this thesis.

DEDICATION

I dedicate the thesis work to my parents for their supportive role, and motivation they provided me throughout my M.Sc. degree.

TABLE OF CONTENTS

LIST OF TABLES

LIST OF FIGURES

CHAPTER 1. MOTIVATION & BACKGROUND

Thermal spraying is a convenient method for rapid deposition of protective layers on the surface of parts, components, and structures. A wide choice of coating materials, including ceramics, alloys, metals, some type of polymers and carbides can be deposited using thermal spraying coating. Coatings fabricated by thermal spraying techniques are increasingly finding application in aerospace, automotive, biomedical, electrical, and turbine industries. Usually industries use thermal spray coatings because they offer improved:

a) Heat resistance

b) Wear resistance

c) High-temperature oxidation protection

d) Fretting and erosion resistance

e) Electrical properties (resistance and conductivity)

f) Corrosion and oxidation properties

g) Electromagnetic properties (Radio-frequency shielding)

Thermal spraying techniques can be categorized based on their energy sources. Flame spray, wire arc spray and plasma arc spray are the three major energy source's categories. In thermal spraying techniques the energy is consumed in order to heat the coating materials to semi-molten or molten state [1]. For example wire arc spray technique uses an electric source or detonation gun uses chemical compounds for heating up the coating materials. Typically the coating materials are in the form of wire, rod, or powder. Thermal spray techniques are explained in detail in chapter 3.

Mechanical properties of the coatings fabricated by thermal-spray coating are mainly based on their microstructure characteristics, morphology, and interfacial properties between splats. During deposition and solidification process, molten particles known as “splats” form interlocked lamella type structures. Usually, the grains grow across the thickness of the splats and often oriented in the direction of the temperature gradient [2]. The pancake-shaped splats are the basic structural units of a coating [3]. Some unwanted phases such as oxides, and voids would associate within the coating structure during the coating process [4]. Therefore, proper characterization of coating materials will significantly improve understanding of critical microstructural features which affect the physical and mechanical properties of coating structures. There is a huge need to develop an efficient microstructural based scheme to evaluate mechanical properties of coating materials. There is a significant difference between the properties of as-sprayed deposits and the fully dense materials.

It has been a big challenge for engineers and researchers to experimentally characterize mechanical properties of coating materials as free standing samples. There are some limitation for capturing the mechanical properties of coatings using methods such as tensile test due to very thin thickness (100μm-500 μm) of them, and the fact of difficulty in separating the coating layer from substrate. Therefore the coating structures usually must be characterized as they stand on their substrate.

Generally, coatings are considered anisotropic and heterogeneous materials which exhibit different properties at different directions respect to the spraying direction. Due to the problems with experimentally measuring of mechanical properties of coating structures, it has been tried to develop an analytical method to predict of mechanical behavior of coating structures independent of experimental tests. There are a few published theoretical papers that have studied and

described the relationships between the mechanical properties and microstructural characteristics of coating structures 5-7. However, thermal spray coatings exhibit a complex lamellae type microstructure. Thus, forming a convenient relationship between microstructural and mechanical characteristic of an as-sprayed coating is a challenging issue. These studies only take into the account the volume fraction of the pores and voids in the coating microstructure. Models have also been developed to establish the same relationship for MMCs processed via conventional techniques such as casting and powder metallurgy [8,9]. Some studies proposed a microstructure-based finite element analysis to predicting the mechanical properties of particle-reinforced metal matrix composites [10-13]. However, no model can claim a complete success in accurate estimation of the mechanical properties of coatings [14].

This research tries to evaluate mechanical properties of thermal spray coatings based on their microstructures characteristics. Theoretical equations were applied to evaluate the Young's modulus of porous materials, and composite materials in term of microstructural features. Moreover, Object Oriented Finite element analysis (OOF) is performed on the microstructure image of thermal spray coatings in order to calculate their Young's modulus. To validate results obtained from analytical models and numerical simulations, experimental studies such as Knoop hardness test and Resonant Frequency are performed on the freestanding coating samples. Comparison between the obtained results from experimental studies, theoretical models, and finite element simulations gives us better understanding of the effect of microstructural characteristics on the mechanical behavior of Alloy 625 and aluminum composite fabricated by deposition technique.

Two different deposition systems were employed to spray different materials to increase the validity of the results in this study. Copper particulate-reinforced aluminum matrix composite

produced by cold spraying and Alloy 625 super-alloy deposited using wire arc spray technique, were studied in this research. Aluminum matrix has been reinforced with 10% and 20% copper particles by volume. A composite made from aluminum and copper will be a suitable choice for materials deposited using cold spraying technique due to high ductility of these materials. In addition, the availability and low cost, made them more attractive to be used in our study. Wire arc spray is a flexible, rapid, and relatively inexpensive method for deposition of metallic materials which can be formed in the form of wire. It requires minimal facilities compared to the other thermal spraying techniques. Deposition of high strength coating on the surface of large structures is possible using this versatile and potable technique. Due to these advantages and the availability of this technique, Alloy 625 coating was deposited using wire arc spray process in this study. Nickel based superalloys outperform other high temperature materials like iron based superalloys, because they are known for exceptional oxidation resistance at high temperatures, exceptional toughness and ductility, and are relatively cheap to manufacture.

CHAPTER 2. LITERATURE REVIEW

A fair number of researches have investigated mechanical properties of thermal sprayed materials. They have tried several methods, such as experimental, analytical, and computational simulation were introduced to determine the elastic modulus, microhardness, fracture toughness, and other physical and mechanical properties of coating structures.

Some other experimental methods such as tensile test have been applied on coating structures in order to determine the elastic modulus. Azarmi et al. measured the Young's modulus of Air Plasma Sprayed (APS) Alloy 625 and studied the relationship between microstructural characteristics and mechanical properties in this type of coating structure [14]. Although they have reported very interesting results, but the mechanical testing and sample preparation looks very difficult, costly, and time consuming process. First, the coating specimens were separated from the substrate and then tensile specimens were sliced to required dimensions using an electric discharge machine (EDM) according to the ASTM B533-85.Due to the very small thickness of the coating deposition (300-600 μm) and size limitations they could only prepare limited number of sub-sized tensile test samples for their experiments. To eliminate the residual stress during machining process samples were have heat treated at 899ºC. Finally they have reported the results for tensile test of as-sprayed, heat treated, and conventionally processed (bulk) Alloy 625 as shown in Table 1. They have concluded the main reason for the significant drop in the mechanical properties of coatings comes from the weak bonding between the splats of the coatings. Moreover the voids and secondary phase such as oxides contributes in low Young's modulus of coating material [14].

Table 1. Tensile test results for mechanical properties of APS deposited Alloy 625 (Azarmi et al, 2009).

Specimen (Alloy 625)	Yield strength (MPa)	Strain at break (%)	Load at break (N)	Young's Modulus
Bulk	320	15-20	-	205
As-sprayed	140±15	1.3±0.1	257±11	20±1
Heat treated (1 h)	225±15	1±0.1	323±23	25±5
Heat treated (3h)	230±20	1.3±0.1	445±29	35±2
Heat treated (5h)	305±10	1.5±0.1	670±14	44±3

Van Steenkiste *et. al.* performed a wide study on aluminum coatings prepared via kinetic spray technique [15]. As a result in this study the mechanical properties, such as Ultimate Tensile Strength (UTS), hardness, and elastic modulus of as-sprayed and bulk type of aluminum is measured and compared. The Young's modulus of the as-sprayed free standing aluminum coating was found to be 55-57% lower than the one reported for bulk aluminum. However, the measured UTS and yield strength of aluminum coating were comparable to those of bulk aluminum.

Marshall et al. proposed a unique method for measuring Young's modulus (E) and hardness (H) [16]. In this technique the measurement of elastic modulus is based on the change in the length of the minor and major diagonals of the in-surface knoop indentations $2b'$and $2a'$, respectively, after elastic recovery. As shown in Figure 1 a diamond pyramid shape indenter is used in this technique.

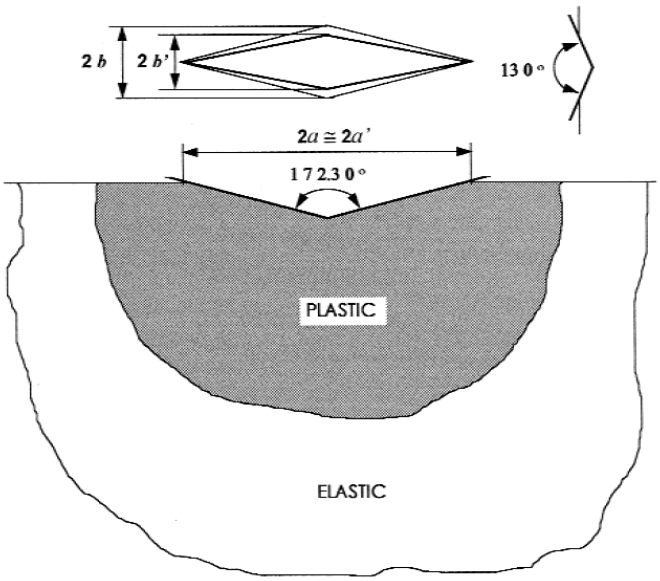

Figure 1. Elastic recovery of Knoop indentation impression and model for elastio–plastic indentation (Lawn. et al, 1981).

In the entirely loaded state, the ratio of the major and minor diagonals is a'/b'=7.11 which is defined by the indenter geometry [16]. The following equations relate the displacement of the minor diagonal 2b and H/E:

$$b - b' = \frac{\alpha a p}{E} \tag{1}$$

$$a - a' = \frac{\alpha b p}{E} \tag{2}$$

$$\frac{b\prime}{a\prime} = \frac{b\prime}{a} = \frac{b}{a} - \frac{\alpha H}{E} \tag{3}$$

The knoop hardness can be calculated using the following equation:

$$HK = \frac{1450 \times F10^3}{b^2} \tag{4}$$

Marshall and Conway proposed the following elastic-plastic equation, based on Lawn and Howe's theory [17], which could be used to obtain the hardness and Young's modulus of the material.

$$\left(\frac{b\prime}{b}\right) = 1 - 2[(1-\nu^2)tan\gamma]\left(\frac{H}{E}\right) \quad (5)$$

where ν is the Poisson's ratio, E is the Young's modulus, 2b and $2b'$is the minor diagonal length before and after recovery, respectively, and γ is the average half-angle of a Knoop indenter, 75°. Eq. X can be rearranged in terms of elastic modulus as follows:

$$E = \frac{\alpha_1 HK}{(\frac{b}{a}-\frac{b'}{a'})} \quad (6)$$

Where HK is the Knoop hardness, α_1 a proportionality constant, b'/a' is the ratio of minor and major diagonals after recovery, and *b/a* is the ratio of minor and major diagonals in the fully loaded state, respectively, given by a constant 0.140646. The main advantage of this technique compare to the other hardness techniques is the capability of determining the elastic modulus and hardness simultaneously. In addition because of the small size of indenter several hardness measurements can be done on a small specimen. Due to the shape of Knoop indenter it covers large area including coating, splat boundary, and voids.

Sang-Ha Leigh et al applied Marshal equation to measure elastic modulus of alumina with different composition using air plasma spray, and water-stabilized plasma techniques [18]. They found that APS produced samples show lower elastic modulus value compare to the ones fabricated by water-stabilized plasma (WPS) spray technique. They have also found that elastic

modulus of the Vacuum Plasma Sprayed (VPS) nickel aluminide exhibit higher elastic modulus compare to the Wire Arc sprayed one.

Another experimental study tried to measure the elastic modulus of tungsten coating deposited by VPS technique using flexural bending test. Bending stiffness (S_b) and tensile stiffness (S_t) were calculated from [19, 20]:

$$S_b = \frac{1}{3}[E_c^* h_c^3 + E_s^*(h_t^3 - h_c^3)] - S_t \delta^2 \quad (7)$$

$$S_t = E_c^* h_c + E_s^* h_s \quad (8)$$

$$\text{With } \delta = \frac{1}{2S_t}[E_c^* h_c^2 + E_s^*(h_t^2 - h_c^2)] \quad (9)$$

$$\text{And } E_s^* = \frac{E_s}{1-\vartheta_s^2}, \quad E_c^* = \frac{E_c}{1-\vartheta_c^2} \quad (10)$$

Where h is the thickness and the subscription *t, c,* and *s* represent total, coating, and substrate respectively. According to the three points bending test criteria the total bending stress equation (Eq.7) could be simplified as follows:

$$S_{b3} = \frac{P_3 l^3}{48 w_3} \quad (11)$$

Where P_3 and w_3 are the total bending force and the maximum deflection, respectively.

In a four point bending test case the total bending stress could be obtained from Eq. 12 & 13:

$$S_{b4} = \frac{P_4 l_o (3l^2 - 4l_o^2)}{48 w_4} \quad (12)$$

$$S_{b4} = \frac{P_4 l_i^2 l_o}{16 w_{4,r}} \quad (13)$$

By applying the rule of mixture to the bending force-deflection the coatings Young's modulus could be calculated as follows:

$$E_c = \frac{P_3 l^3}{4bh^3 w_3} \cdot \frac{h_c}{h_c + h_s} \tag{14}$$

The Young's modulus obtained for tungsten coating was approximately 14% of the bulk tungsten young's modulus (400GPa). Also the literature indicates that usually the elastic modulus of tungsten coating fabricated by plasma-sprayed technique is 20-30% smaller that its bulk elastic modulus.

Li *et. al.* determined the Young's modulus of hydroxyapatite (HA) coating using indentation test along with three- and four-point bend test [21]. The elastic modulus values determined by Three- and four-point bend tests indicates a higher Young's modulus for coatings prepared with a larger HA powders, and the improvement of elastic modulus values after heat-treating the coating samples. They have concluded that the elastic modulus result of the bio-ceramic coatings is considerably related to the microstructure morphology and phase composition. However, there were significant errors for the elastic modulus obtained from indentation technique. These results indicated that indentation test was impacted by the surface roughness of coating samples and basically it is a local-phase-dependent technique not very appropriate for bulk elastic modulus calculation. It is found that bend tests were more reliable for characterizing the elastic modulus of coatings and the good agreement between the results determined from three point bend test and four point bend test.

H-J. Kim and Y-G. Kweon, have investigated the young's modulus of number of metallic, cermet, and ceramic coatings fabricated by plasma-sprayed techniques using three-point bend test [22]. As a result Ni20Cr (B1) and Co32Ni21Cr8Al0.5Y (B2) are the two metallic

coatings used in this study. In addition they have conducted Knoop indentation technique to obtain the hardness and Young's modulus on the coatings. Since the splat boundaries, pores, and oxide layers in the planer- section (perpendicular to the deposition surface) is higher than the cross-section, the obtained elastic modulus for both materials was to be found lower in planer-section. It has been mentioned in thermally sprayed coatings structures the major difficulty of determining the elastic modulus is the problem in capturing the pure elastic deformation. The main problem appears during the mechanical tests when movement of splat boundaries and/or propagation of cracks affect the Young's modulus value. Therefore, due to this phenomenon in thermally sprayed coatings the obtained elastic modulus would be also dependent on the applied technique and measurement. Since the three-point bend test takes to account this phenomenon and as the Knoop technique only considers the elastic region in evaluating elastic modulus, the determined values for elastic modulus from this three-point bend test (for coatings with 10% porosities) seems to be lower compared to those obtained from Knoop hardness test.

Gross *et. al.* performed nanoindentation test on hydroxyapatite (HA) produced with Powder Plasma Sprayed (PPS) and Suspension Plasma Sprayed (SPS) techniques [23]. The intent of this study was to investigate and compare the mechanical properties of the same coating materials fabricated with different techniques. The elastic modulus of the coating prepared by SPS shows a higher value than the PPS coating. They have concluded the coatings fabricated by SPS contain more porosity than the PPS coatings, which would lead in lower elastic modulus and hardness. But due to the crystal orientation and finer grain size in the SPS coatings compare to the PPS coating the elastic modulus and hardness values were slightly greater.

Singh *et. al.* have evaluated the Young's modulus of an Yttria Stabilized Zirconia (YSZ) Thermal Barrier Coating (TBC) using Knoop indentation technique [24]. Also they have

measured the hardness by Knoop and Vickers indentation techniques. They have concluded by increasing the load the elastic modulus and hardness would decrease. The values obtained from knoop and Vickers technique were in good agreement. Azarmi et al. have also used three theoretical models to determine the Young's modulus of coating according to its microstructural characteristics. The first applied model was Sprigg's equation, which is a commonly used empirical equation for porous materials [25].

$$E^* = E_s \exp(-bp) \tag{15}$$

where P is known as the volume fraction of all voids, splats interfaces, and cracks. By substituting the above values, the estimated E^* was found to be 166 GPa.

Hashin-Hasselman is one of the most common models used to estimate the mechanical properties of porous materials . The estimated Young's modulus by Azarmi *et. al* for APS Alloy 625 using Hashin-Hasselman equation [26, 27] is 85GPa. The Zhao model [28, 29] was the last analytical model used by them to predict mechanical properties of the APS Alloy 625 coating which is capable of measuring elastic modulus in both transverse and longitudinal directions.

$$E_L = \frac{E_m(1-p)}{1+2n\rho} \tag{16}$$

$$E_T = \frac{E_m(1-p)}{1+2\pi\rho\alpha^{-2}} \tag{17}$$

Where p is the volume fraction of elliptical voids, ρ is the total volume fraction of voids and oxides, E_L, the longitudinal Young's modulus (perpendicular to coating plane), E_T, the transverse

Young's modulus (parallel to coating plane), and E_m is the Young's modulus of the bulk material. The obtained values were 105 and 141GPa for the longitudinal (E_L) and transverse (E_T) directions, respectively.

Table 2. Analytical models predictions, Objective Oriented Finite Element Analysis (OOF) calculation, and experimentally measured Young's modulus for as-sprayed and heat treated samples (Azarmi et al, 2009).

Method		Strain at break %	E_t,transverse (GPa)	E_L,longitudinal (GPa)
	Sprig as-sprayed	-	166	-
	Zhao as-sprayed	-	141	105
	Hashin-Hasselman as-sprayed	-	85	-
OOF	As-sprayed	-	49	25
	Heat treated 5 (h)	-	64	31
Tensile test	As-sprayed	13	20	-
	Heat treated 5 (h)	13	44	-

Azarmi et al have reported a 90% reduction in the elastic modulus of as-sprayed Alloy 625 fabricated by plasma spray technique compare to the conventionally fabricated Alloy 625, shown in Table 2 [14]. The main reason mentioned is due to the weak bonding between the splats in the coating structure. Also the predicted elastic modulus from the analytical models such as Sprigg's model was so far away from the tensile test results.

Hashin-Shtrikman (H-S) and Halpin-Tsai (H-T) both proposed empirical and semi-empirical models for calculating the elastic modulus of composite materials [8, 30]. According to the H-T equation, the discontinuous reinforcement particles are assumed to be oriented perfectly in the composite and parallel to the applied load. The H-T model could be written as follows for calculating the elastic modulus:

$$E_c = \frac{E_m(1+2sqV_p)}{1-qV_p} \tag{18}$$

Where E_p is the elastic modulus of the reinforcement phase, E_m is the elastic modulus of the matrix phase, E_c is the elastic modulus of the composite, s is the aspect ratio of the particles, and q is given by:

$$q = \frac{(\frac{E_p}{E_m} - 1)}{(\frac{E_p}{E_m} + 2s)} \tag{19}$$

Both results obtained from Hashin-Shtrikman and Halpin-Tsai over predict the Young's modulus of the MMC. Obviously these analytical models are not able to capture the microstructure features that affect the mechanical properties of the composites. The above mentioned analytical models were used in this study to determine elastic modulus of the deposited materials. The details can be seen in chapter 5.

Several theoretical models are available to determine the elastic properties of materials respect to their microstructural features. Sprigg's [25] suggested a model to measure mechanical properties of transversely isotropic materials as follows:

$$E = E_0 \exp(-b_e P) \tag{20}$$

Where b_e is a constant (~2) [31], E_0 the Young's modulus for a zero-voids material, and P the voids volume in the material.

Rossi [31] has proposed a mathematical expression to estimate the elastic modulus of materials with spherical porosities. The model is based on the microstructural models of composite materials, which the shape of the included phase is considered as well as the moduli of the individual phases as follow:

$$E = E_0[1 - \left(\frac{5a}{4c} + \frac{3}{4}\right)P] \quad (21)$$

Where E_0 is the Young's modulus for a zero-voids material, c is the parallel axis to stress direction, and a is the perpendicular plane axis to axis c.

Since, coatings are considered as anisotropic materials, it is assumed that the mechanical behaviors are not the same at different directions. Sang-Ha Leigh et al have performed mechanical tests in directions parallel (*longitudinal*) and perpendicular (*Transverse*) to the spraying deposition plane. As shown in Table 3 the mechanical properties are considerably different for the coatings in different direction, where M2 and M6 are nickel-aluminum and Cr2C3-NiCr, respectively, and both fabricated by Arc Plasma Spray (APS) technique.

Table 3. Young's modulus results parallel and perpendicular to the deposition surface (Sang-Ha Leigh *et al*, 1997).

				Elastic modulus data		
Sample	Load (kg)	Direction	*H/E*	Mean *E* (GPa)	*m*	$E_{\parallel}/E_{\perp}$
M2	0.5	$E_{\parallel}$	0.03756	30±11	3.1	1.5
M2	0.5	$E_{\perp}$	0.05807	20±6	3.6	1.5
M6	1	$E_{\parallel}$	0.03435	175±34	5.0	1.5
M6	0.5	$E_{\perp}$	0.05657	93±14	6.2	1.5

Since the microstructure has a huge effect on the physical and mechanical properties of a coating materials, it is important to take to the account all microstructure features to determine these properties. Although the complex coating microstructures often makes it difficult and challenging to determine the mechanical properties by using numerical technique, an image based Finite Element Analysis (FEA) software, known as Objective-Oriented Finite Element (OOF) software can be used to numerical simulation of coating microstructures. This program

uses the actual micrograph and incorporates the microstructural data with the fundamental material data (i.e. elastic modulus and Poisson ratio) for predicting of the mechanical properties.

Chawla *et. al*. have applied OOF for predicting the mechanical properties of SiC particle-reinforced aluminum matrix composite and double-cemented WC particle-reinforced Co matrix composite based on their microstructures [32]. The SiC-Al composite was fabricated via Powder Metallurgy (PM) processing and extrusion and the WC-Co composite produced by a Rapid Omni-directional Compaction (ROC) technique. In this study they have observed a better agreement between the values obtained from OOF to the experimental techniques compare to analytical ones. They have concluded OOF can be applied as an effective tool for predicting the mechanical properties of materials. Also it is an effective program for studying the microstructure effect on the localized stress state [32].

Azarmi *et. al.* have also used OOF program to obtain the elastic modulus of APS Alloy 625 coating [14]. The obtained elastic modulus in the transverse and longitudinal direction was 49 and 25 GPa, respectively. These results are 150% higher than the results obtained from tensile test (20Gpa) in the transverse direction. They have concluded a significant difference between the obtained values from experimental and numerical techniques, due to the failure of OOF in capturing all microstructure features which has a strong influence on the mechanical properties [14].

Several studies have been done on simulation of three-dimensional (3D) metal matrix composite's (MMCs) microstructures. Chawla *et. al.* have developed a 3D model of the microstructure of SiC particle reinforced Al composite and studied the mechanical behavior of the composites using finite element analysis (FEA) [11]. They have modeled the MMC by using serial sectioning process as shown in Figure 2.

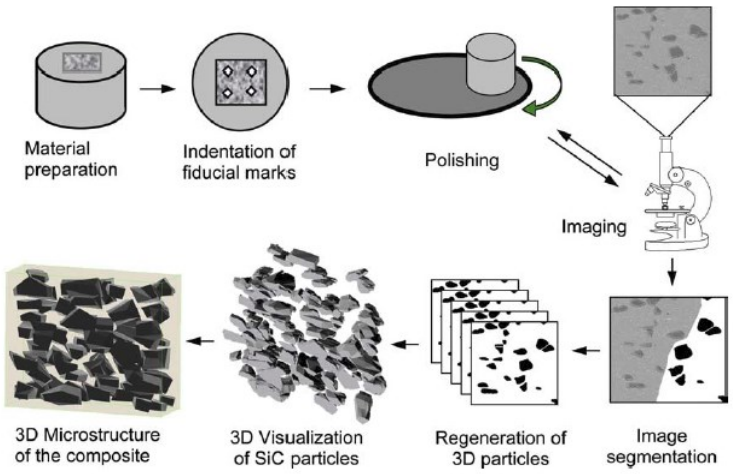

Figure 2. Flow chart of several sectioning and 3D reconstruction process (Chawla *et al,* 2006).

The slicing technique combined with FEA seems to be a good improvement over 2D models used by programs such as OOF. There is a good agreement between results obtained from 3D microstructure-based model and experimental tests. Nonetheless, the microstructure-based 3D reconstructed models represent very close results to the experimental response, 3D reconstruction process is a costly technique and it requires huge increase of processing time due to the large number of elements in the 3D microstructure-based model which require additional refinement of the meshes before solution. The highest elastic modulus and strength from the simulation were obtained by prism unit cell model and the lowest values were obtained by sphere unit cell model. This can be caused due to the higher degree of load transfer for the perfectly rectangular unit cell's particle compare to the spherical unit cell's particle. Comparing the sphere and prism unit cell 3D model results with the experimentally obtained elastic modulus shows a good correlation. As a result the perfectly rectangular unit cell, microstructure-based models and experiment stress-strain curve were approximately fitted.

None of those studies tried to compare results of mechanical evaluation from different methods. We are planning for a more comprehensive study by performing analytical,

experimental, and numerical techniques to determine the mechanical properties and comparison of the results to develop an effective model to predict mechanical properties of coating structures.

CHAPTER 3. THERMAL SPRAYING TECHNIQUE

Thermal spraying techniques are well-established methods to deposit metallic or nonmetallic hard coatings. In this technique the particles in molten, semi molten or solid condition are sprayed with high velocity toward the substrate, resulting in formation of a coating layer on the surface of the substrate. The speed of droplets or particles is in the range of 50 to 1200m/s. Significant amount of deformation of the particles can occur during impact due to high speed and high temperature. Impacted particles on the substrate are called “splats” which are considered as building blocks of any coating [1]. Each splat flattens and solidifies on the substrate where cooling rate during solidification is an important parameter in morphology and properties of coatings. A rapid cooling rate generally results in a fine structure. Coating layers are formed by deposition of splats on top of each other building coating structure. Figure 3 shows a schematic of thermal spraying technique and coating build up process. Thermal spraying technique has several distinct advantages compare to traditional methods such as powder metallurgy (P/M). These advantages are listed as follows:

1. A wide variety of materials can be deposited in this technique (typically, any material that does not decompose in its melting point could be sprayed).
2. Some techniques such as wire arc and cold spraying could deposit coatings with minimum heat input to the substrate. The flexibility of the techniques to repair damaged parts without replacing or changing the structure or dimensions of components.

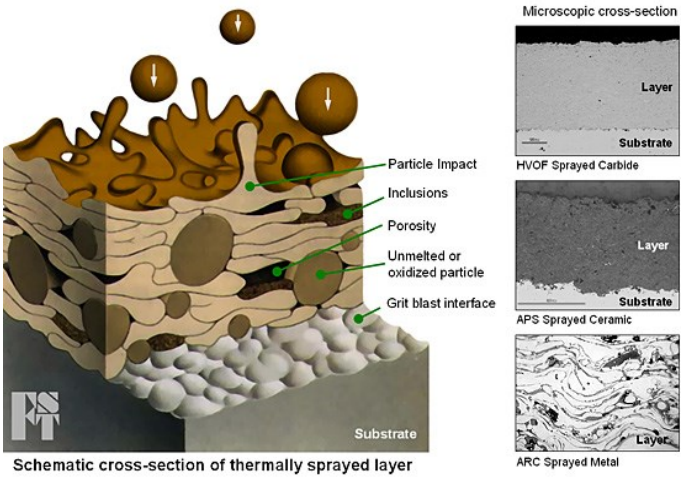

Figure 3. Schematic cross-section of thermally sprayed layer and as-sprayed coating microstructures [http://www.gordonengland.co.uk/tsc.htm].

The main disadvantage of this technique is the line-of-sight limitation which makes it difficult for coating complicated shapes [1].

Thermal spraying technique could also be used to deposit coating from high temperature materials such as tungsten, and ceramics. Moreover this method is more flexible for applying coating on complex structures, and requires shorter time for deposition of protective layer on the surfaces. Due to the above mentioned advantages; Thermal spraying seems to be a promising route for fabrication of metal matrix composite (MMCs). The powder mixture of desired constituents can be deposited to form a composite structure. Thermal spray technique has found several applications were protection against oxidation, wear, thermal shock, and corrosion is required, and application in industry areas, such as petrochemical, gas turbine blades, and medical implants [33,34].

Thermal spray processes can be grouped based on their energy sources into two categories: combustion or electrical sources (in order to melt or soften the particles). Typically selection of an appropriate thermal spray technique is determined by [1]:

1. Fabrication costs
2. Coating material
3. Application
4. Substrate geometry and material

Some common commercial thermal spray techniques and their specs are listed in Table 4:

Table 4. Comparison of thermal spray techniques (Adopted from Brendt and Lenling, 2004).

Process	**Gas flow (m^2/s)**	**Flame temperature (°C)**	**Particle impact velocity (m/s)**	**Cohesive strength**	**Oxide content**	**Relative process cost**	**Energy required to melt (kw/kg)**
Flame powder	11	2200	30	Low	6	3	11-22
Flame Wire	71	2800	180	Medium	4	3	11-22
High velocity oxyfuel	28-57	3100	610-1060	Very high	0.2	5	22-200
Detonation gun	11	3900	910	Very high	0.1	10	220
Wire arc	71	5500	240	High	0.5-3	1	0.2-0.4
Conventional plasma	4.2	5500	240	High	0.5-1	5	13-22
High energy plasma	17-28	8300	240-1220	Very high	0.1	4	9-13
Vacuum plasma	8.4	8300	240-610	Very high	(0)	10	11-22

Single-phase and multiphase materials such as alloys, metals, intermetallics, ceramics, and polymers, composite materials such as metal matrix composites, reinforced polymers, and cements and functionally gradient materials (FGMs) can be deposited by thermal spray techniques.

3.1. Cold Spray Coating

Cold spray technique was first technologically advanced at the Russian Academy of Science at mid-1980s by Papyrin and colleagues [1]. Cold spraying is a well-known technology to deposit metal or metal alloy particles as a coating layer on different substrates. The process is based on acceleration of solid particles toward the substrate. Coatings are formed layer by layer after impact of small solid particles (size ranging from 1 to 100 μ m) at high velocities (usually 300 to 1200 m/s) with the substrate [35]. In order to reach this goal, metal powder particles are introduced into a heated pressurized gas flowing via a converging/diverging nozzle to reach a supersonic speed. Due to the impaction process this method is limited to ductile and deformable materials such as ductile metals and polymers. Cold spray is not an appropriate technique for depositing brittle and hard materials such as ceramics as coatings because they will be crashed and shattered during impact. Since in this technique the particles are preheated to low temperatures (300 to 600°C) usually lower than their melting point it has significantly lower deleterious effects of high temperature compare to other conventional thermal spray techniques [36]. As a result in this technique oxidation, melting, recrystallization, residual thermal stresses, decomposition, and evaporation is significantly minimized or eliminated. Coatings fabricated by cold spray technique usually exhibit acceptable mechanical behavior. Figure 4 shows schematic of cold spraying technique.

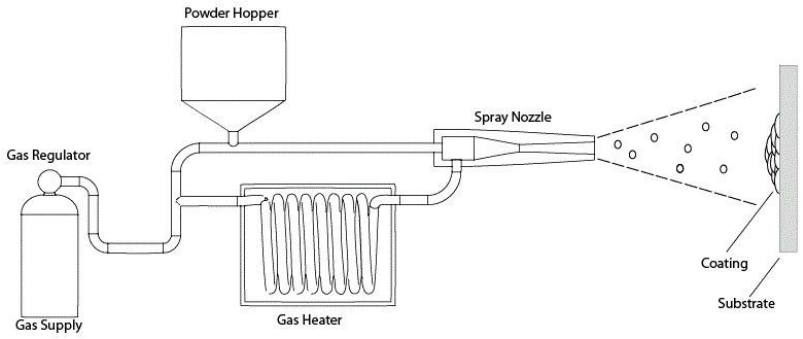

Figure 4. A schematic of a conventional cold spray process (Bashirzadeh *et al,* 2013).

Equipment: Typically a cold spray system consists of the following parts:

1. Extreme high-pressure gas supply (usually nitrogen)
2. Gas control module
3. Gas heater and powder-metering device
4. De Laval-type nozzle (i.e., a converging/ diverging nozzle)
5. Hoses and cables

3.2. Wire Arc Spray Coating

This technique was originally proposed by M.U. Schoop in 1910, but it did not find considerable commercial application until 1960s. In this technique the materials are in the form of consumable rods. Unlike other thermal spray techniques this technique applies a direct current (dc) between the rods which results in a formation of an electric arc in the gap between the rod tips as the two rods are continuously consumed together [37]. As shown in Figure 5 the molten particles are then will be accelerated toward substrate by a high velocity air jet (air flow ranges from 0.8 to 1.8 m^3/min) [1].

The thermal efficiency is considerably higher than other thermal spray techniques due to the direct melting process by the electric arc. The other advantage of this technique is the lower cost compare to other coating methods. The oxidation of the molten particles could be minimized by using short standoff distances and high compressed air flows. Generally, coatings fabricated by electric arc spray technique end up with a denser and stronger structure than coatings fabricated by equivalent combustion spray techniques [38]. Since, in electric arc spray technique an electric current is applied to the pre-coated materials (wires); thus, the materials shall be electrically conductive wires to be able to apply them in this technique. The other disadvantages are that a separate heating source is needed for spraying the materials and substrate preheating is required prior and during spraying process. The arc spray process is heavily used in production of anti-corrosion coatings of zinc and aluminum [1,39].

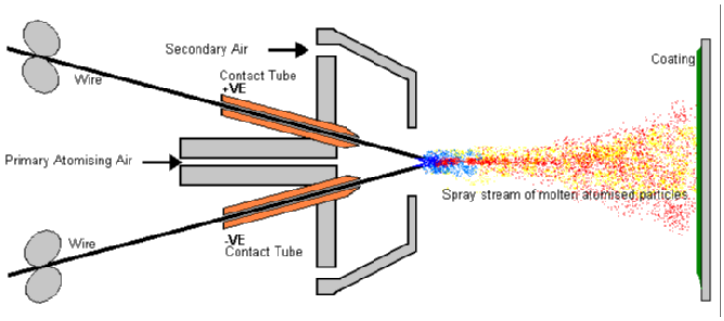

Figure 5. A schematic of a conventional wire arc spray process [http://www.gordonengland.co.uk/xaws.htm].

Equipment: Typically a wire arc spray system consists of the following parts:

1. Pressured air supply
2. Power Supply (constant dc voltage)

3. Wire feeder comprising an electric or air-driven motor, drive wheels, and drive wheel tensioning devices
4. Electric arc spray gun and air nozzle
5. Wire guide/contact tips, air cap, and arc shield.
6. Hoses and cables

In order to improve the deposition microstructure in this technique, using smaller-diameter wires, high velocity air caps (to reduce dwell time), inert atomizing gases (to reduce the oxidation), and lower arc voltage (for minimizing overheat of the droplets) during the deposition process is required.

CHAPTER 4. MATERIALS

4.1. Metal Matrix Composites (MMCs)

MMCs are extensively finding application in aircraft components, automotive industry, cutting tools, and sporting goods [10]. MMCs can be classified into three main groups:

1) Discontinuously Reinforced Metal Matric Composites (DRMMC) such as particle reinforced MMCs.
2) Fiber Reinforced Metal Matrix Composites (FRMMC):
   - Short fiber reinforced MMCs or, rather, whiskers composite.
   - Continuous fiber reinforced MMCs, such as mono filaments composite.
3) Layer Metal Matrix Composites (e.g. mono filaments) [40].

Some examples of particle and fiber reinforced MMCs have been illustrated in Figure 6 [41].

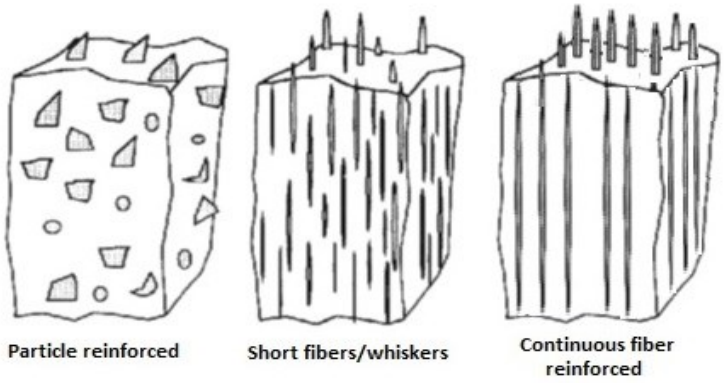

Figure 6. Schematic of different types of MMCs [T. W. Clyne et al, Cambridge 1993].

Reinforcing elements were added to the metal matrices to obtain materials with higher thermo-mechanical and electrical properties such as wear resistance, fatigue strength, creep resistance, corrosion resistance, thermal conductivity, electrical conductivity, high stiffness, high

strength, and performance at elevated temperatures [40, 42]. MMCs can be manufactured by one of the following techniques:

1. Squeeze casting
2. Physical vapor deposition
3. Stir casting
4. Electroplating / Electroforming
5. Powder metallurgy
6. Foil diffusion bonding
7. Spraying deposition

MMC was chosen in this study due to their isotropic properties, cost-effectiveness, and significantly improved properties over conventionally fabricated metals, such as higher strength, stiffness, and weight savings. Particularly aluminum matrix composite with incorporation of copper was chosen due to its low weight and availability, in addition to its compatibility to be fabricated by cold spray coating technique. The distinct properties of Alloy 625 in high service temperatures such as high creep, static, and fatigue resistance made it an appropriate case for this study.

4.2. Aluminum Copper MMCs

In particular, aluminum matrix composites are very attractive due to their light weight and high strength to weight ratio. Particulate-reinforced aluminum matrix composites have been used widely for low temperature structural components in the automotive, aerospace and sport industries [1]. In addition particulate-reinforced aluminum matrix composites prepared by incorporation of copper particles offers a combination of strength and high electrical and thermal

conductivity, which has made them attractive for many electrical and thermal conduction applications such as high field magnet technology and electronic circuits [1,36,43,44,45]. Addition of copper to the aluminum considerably improves wear resistance of the aluminum. The two most important advantages of particulate-reinforced aluminum matrix composites when compared to fiber or laminate reinforced composites, are their isotropic mechanical properties and ease of fabrication into complex shapes. All types of reinforcements including SiC, B, B4C, Al_2O_3, ZrO_2, graphite, copper, aluminides, and Kevlar have been investigated for use in aluminum-based MMCs [46]. J. M. Torralba et. al. have applied powder metallurgy (P/M) for manufacturing Al-Cu matrix composites [47]. They have concluded that aluminum MMCs produced by P/M requires a lower processing cost compare to other conventional methods and it's a high versatility technique. Multi-layered Al-Cu MMCs were fabricated by accumulative roll bonding (ARB) process by M. Eizadjou *et. al.* [48]. One advantage of this technique is the ability of fabricating multi-layer Al-Cu composite including homogeneously distributed fragmented copper layers in an aluminum matrix. Meanwhile, in this technique the average thickness of copper reinforced layers can be controlled by changing the ARB cycles. Although all mentioned techniques are suitable for manufacturing Al-Cu composites, however parameters such as melting, recrystallization, evaporation, debonding, and high-temperature oxidation influence the final microstructure of MMCs.

4.3. Aluminum-Copper Cold Sprayed Composites

There is an alternative solution to the above mentioned problem which is using cold spray technique. This technique is a rapid, single-step manufacturing process with less heat input resulting in less oxidation, no recrystallization, and minimum thermal stress build up in the

fabricated metal matrix composites. However, since particles are injected in the solid condition, this technique is limited to spraying of ductile materials only. Aluminum and copper are two ductile materials which makes them suitable candidate to be deposited using cold spraying technique. In this study, particulate-reinforced aluminum matrix composites were prepared by addition of 10% and 20% copper by volume.

4.4. Nickel Based Superalloy

A superalloy is a metallic alloy which can be based on iron, cobalt or nickel. Since the 1940s, superalloys have been developed to work at corrosive environment and high service temperatures in excess of 0.7 of the absolute melting temperature [49-51]. Such extreme conditions commonly exist in gas turbines and aeroengines. Creep and oxidation resistance are the prime design conditions for superalloys. Typically nickel is used as the base composition for superalloys due to their high melting point and stability until melting point. Additionally, diffusion rate is low in nickel which limits the creep of nickel based superalloys [51]. From the chemistry prospect the Face-Centered Cubic (FCC) crystal structure of nickel confers the key advantage of the superalloys: Since, this structure would result in substantial ductility and toughness in materials, they are greatly appropriate for engineering applications. Furthermore, materials withFCC crystal structure are very steady and stable from the room temperature to the melting temperature – for pure nickel this lies at 1455ºC. Nickel-based superalloys have been extensively applied in gas turbine engines, rocket motors, submarines, petroleum equipment, and other challenging environments, including nuclear power plants. Typically nickel-based superalloys include 40-50% of the total weight of an aircraft engine. During the past few decades a significant process improvement activities have been resulted in superalloys that can withstand

temperatures to 1050ºC and with occasional excursions as high as 1200ºC, which is approximately 0.9 of the melting point of the material [52, 53].

4.5. Alloy 625 Coating

Alloy 625 is a matrix stiffened super-alloy, with a nickel-based composition containing significant amounts of chromium and molybdenum. The first development of Inconel Alloy 625 was started by H. L. Eiselstein *et. al.* in the 1950s. The main goal was to develop a nickel base composition alloy as a main stream-line material for super critical stream power plants with high creep resistance, weldability, fabricable into tubing, non-agehardening, and have attractive ASME boiler code design. They were able to meet the goal, except for weldability. The developed Alloy 625 composition by H. L. Eiselstein et al is listed in Table 5.

Table 5. Inconel Alloy 625 typical composition (%) [H. L. Elselstein et al, 1991].

Elements	Ni	Cr	Mo	Nb	Fe	Al	Si	Ti	Mn	C	S	Total
Wt %	61	21.5	9	3.6	2	0.2	0.2	0.2	0.2	0.05	0.001	100

Due to the exceptional properties of Alloy 625, such as oxidation resistance at high temperatures, high ductility and toughness, and relatively cheap to manufacture they are an attractive candidate for high service temperature and stress applications, such as aircraft engines and gas turbines, where the temperature excess 650ºC and the mechanical stresses are high, as well. In addition, these types of materials have significant resistance to various applied loads such as static, creep, and fatigue. In the few past decades several studies have been done on improving the mechanical properties of Alloy 625 by adding or adjusting the components.

In this study Alloy 625 coatings were fabricated by wire arc spraying technique. This technique uses two wire electrodes made of the desired coating material. Once an electric arc forms between converging wires, liquid droplets are formed by the produced heat. The droplets are blown by atomizing gas which propels fine particles towards a substrate. Finally the impacted molten particles on the substrate quickly solidify and form the coating structure.

4.6. Alloy 625 by Wire Arc Spraying

In this study, wire arc spraying technique is employed to fabricate Alloy 625 coating. In general, coatings fabricated by wire arc techniques require less fabrication equipment and subsequently lower manufacturing cost. In addition coatings fabricated by this technique are normally denser and have a better bonding between splats than their equivalent combustion spray coatings. Due to the mentioned advantages wire arc spray seems to be an appropriate technique for fabricating Alloy 625 coatings. In this study the mechanical properties of Alloy 625 coating has been examined. In another study the same coating material was deposited on wrought Alloy 625 substrate using wire arc spray technique by Azarmi, et al [54]. The influence of the fabrication technique and solidification rate on the grain size has been observed by comparison between the microstructure of the wire arc sprayed Alloy 625 coating and the bulk Alloy 625 substrate.

The intent of this study is to examine the mechanical properties of wire arc sprayed Alloy 625 coatings. Proper characterization of coating materials will significantly improve understanding of critical microstructural features which affect the physical and mechanical properties of coating structures. The results will be used to relate the elastic modulus, E, of the coating materials to the microstructure. Thermal spray coatings exhibit a complex lamellae type

microstructure. Thus, forming a convenient relationship between microstructural and mechanical characteristic of an as-sprayed coating can be an important tool for further study on coating structures.

CHAPTER 5. EXPERIMENTAL TECHNIQUES

5.1. Al-Cu Cold Sprayed Coating Preparation

Commercially available powder of Al 99.5 % with the irregular shape and the nominal particle size in the range of -45 to +5μm, Centerline (Windsor) Limited, ON, Canada was used in this study. The aluminum particles were mixed with 10% and 20% copper particles (Cu 99.7%) by volume with irregular shape and the nominal particle size in the range of -45 to +5μm, Centerline (Windsor) Limited, ON, Canada. Fabrication of the metal matrix composite samples, consisted of aluminum matrix reinforced with various amounts of copper particulates achieved using the cold spraying technique. The mixture of the Al-Cu particles was deposited on aluminum substrate 130mm×75mm×10mm in size. Bonding of particles is resulted due to the widespread plastic deformation and interlock at the interface boundaries [1,36]. Here, powder mixture was cold sprayed using SST-P Series cold spray system by Centerline (Windsor) Limited, ON, Canada using the parameters shown in Table 6.

Table 6. Operational spraying parameters.

Process Parameters	Value
Temperature (ºC)	350
Pressure (psi)	250
Nozzle Stand-off (mm)	10
Gun Traveling Speed (mm/s)	20
Processing Gas	N2

5.2. Alloy 625 Coating Preparations

In this study commercially available Alloy 625 wire from Oxford® Alloys, Inc was used. The present composition for Alloy 625 wire used as feedstock in this study is listed as Table 7. Alloy 625 coating was deposited using a ValuArc 200 Electric Wire Arc spray gun (Sulzer-Metco, Westbury, NY, USA). Spray parameters applied in tests are listed in Table 8. In order to fabricate an Alloy 625 coating with minimum porosities and secondary phases, such as oxide phase, the spraying parameters applied in this study were chosen from a series of spray runs with different spraying parameters. The substrate used in this study consisted of 100mm×50mm×2mm coupon of Alloy 625. The coating thickness was about 1 mm, where the substrate temperature during deposition was in the range of 60-480°C.

Table 7. Alloy 625 wire arc sprayed composition (%).

Elements	Ni	Cr	Mo	Nb+Ta	Fe	Cu	Mn	Si	Al	Ti	P	S	Total
Wt %	67	20	8	2	0.5	0.5	0.5	0.5	0.4	0.4	0.02	0.015	100

The Alloy 625 coating on the Alloy 625 substrate was sectioned parallel to the spraying direction, mounted, ground, and polished prior to optical microscopy, Knoop hardness testing, and nano-indentation. The samples where mounted in Buehler transoptic powder. Grinding and polishing was completed on Metprep3 PG-3 using 240, 400, 600, 800, 1200, 1600 SiC grit papers for grinding stages, polishing was done using 3 micron diamond suspended solution on Kempad, and final polishing done using 1 micron diamond suspension on Spec-Cloth. A Zeiss Axiovert 40 MAT was used for optical microscopy with iSolution DT as the imaging software.

Table 8. Wire arc spraying process parameters.

Process Parameters	Spray Distance (mm)	Wire Feed Rate (m/min)	Voltage (v)	Atomizing Gas	Air Cap
Value	200	28	33	Dry Air	HV Cap

5.3. Knoop Hardness

Marshall et al. proposed a new technique for measuring elastic modulus and hardness. In this technique the measurement of elastic modulus is based on the change in the length of the minor and major diagonals of the in-surface knoop indentations $2b'$and $2a'$, respectively, after elastic recovery. As shown in Figure 7 a diamond pyramid shape indenter is used in this technique. In the entirely loaded state, the ratio of the major and minor diagonals is $a'/\,b'$=7.11 which is defined by the indenter geometry [16].

As illustrated in chapter 2 (Figure 1) the indentation is formed from a combination of elastic (reversible) and plastic (irreversible) regions. After unloading, the length of the major and minor diagonals of the indentation starts to reduce due to the elastic recovery of the material, whereas the length change in the major diagonal is negligible.

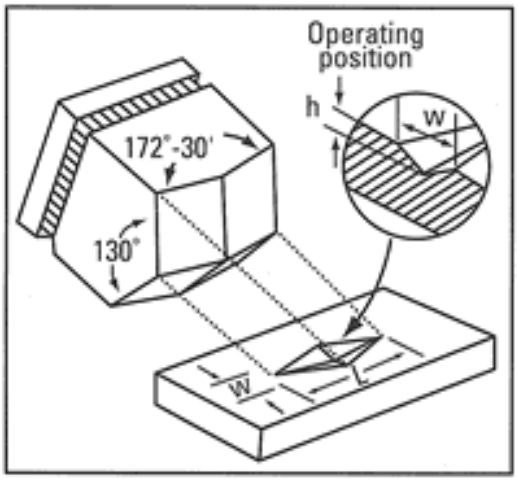

Figure 7. Illustration of the Knoop indenter geometry, also indicating the apex angle of the major and minor diagonals (http://www.instron.us/wa/applications/test_types/hardness/knoop.aspx).

In this study, Knoop hardness experiment was conducted to simultaneously measure the Young's modulus of reinforcement and matrix phases of microstructure in both transverse and longitudinal directions. The Knoop hardness of each sample was measured using a Zwick microhardness machine under an applied load of 9.8 N for 25 s. Nine indentation tests were performed on each coating cross-section, with the long axis of the indent oriented perpendicular and parallel to the deposition direction. The elongated diamond shape covers wide area containing splats, splat boundaries, and voids which makes it suitable for coating structures.

5.4. Tensile Test

The tensile test was conducted on the thermally sprayed coatings to determine the Young's modulus. Tensile Alloy 625 specimens were made from wire arc sprayed Alloy 625 deposited on an Alloy 625 substrate. The coating was separated from the substrate and machined to coincide with ASTM E8M-04 [55]. Due to coating thickness limitations the samples where cut parallel to splat plane also known as the transverse direction. A diagram

of the sub-sized specimen geometry is shown in Figure 8. Tensile tests were performed using a screw-driven testing machine (Instron 5567) at a strain rate of $10^{-4}s^{-1}$ and after fracture tests were ended.

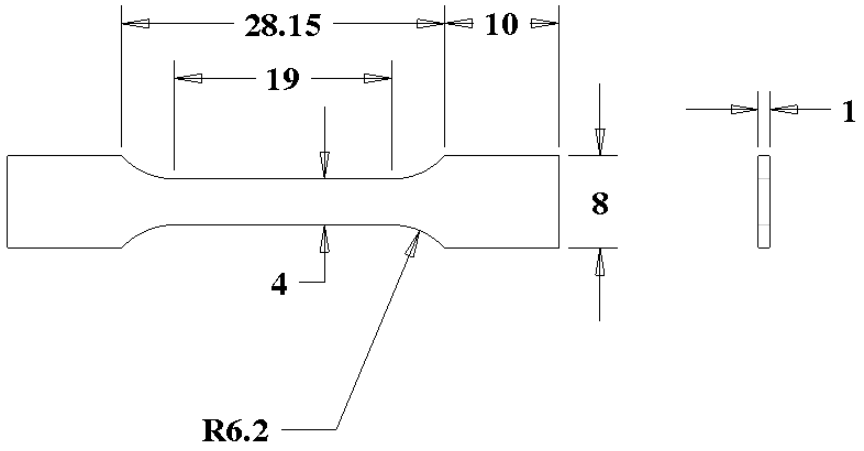

Figure 8**.** Schematic of sub-sized specimen for tensile test (All dimensions in mm).

5.5. Nano Indentation

Nanoindentation technique was developed in the mid-1970s to measure the hardness of small volumes of material [56]. The measurement in this technique consists of two steps, the loading stage and the relaxation stage. Within the loading stage, an indentation load is applied on a hard tip whose mechanical properties are known (usually made from a very hard material like diamond) [56]. The applied load would force the tip to penetrate into the sample [56,57]. As shown in Figure 9 the load placed on the indenter tip is increased as the tip penetrates further into the specimen and soon reaches a user-defined value. During the relaxation stage, the load is taken off from the sample and the elastic recovery would be completed. Depending on the applied load a plastic deformation with a specific depth h_p would remain in the material. In the final stage the Young's modulus could be determined by measuring the maximum penetration

depth and more parameters related to the indentation procedure with an analytical evaluation method.

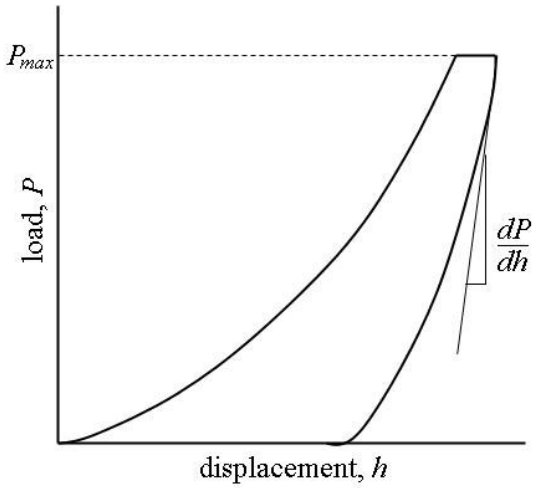

Figure 9. Schematic of load displacement curve for an instrumented nanoindentation test (http://en.wikipedia.org/wiki/Nanoindentation).

5.6. Resonance Frequency

Resonance Frequency technique, also known as Impulse Excitation, is a non-destructive method capable of measuring the elastic properties of a sample continuously at ambient and high temperature conditions. The elastic properties of a coating can be determined by exciting (tapping) a sample with a small hammer and detect the induced vibration signal with a microphone. In the next step, a software package analyzes the vibration signal and determines the sample's mechanical properties such as elastic modulus, shear modulus, and Poisson ratio. Figure 10 shows a schematic of the Resonant Frequency Analyzer set-up used in this study.

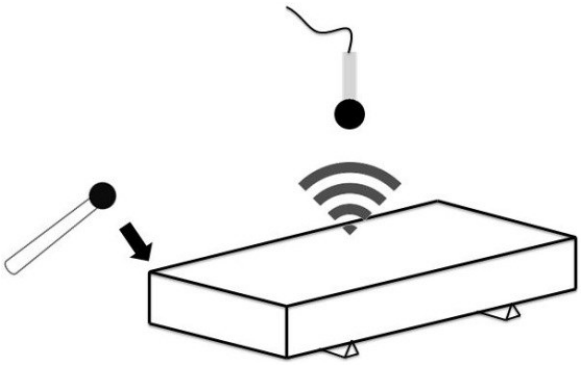

Figure 10. A schematic of a resonance frequency test set-up (Bashirzadeh, *et al,* 2013).

Al-Cu and Alloy 625 samples were subjected to an impulse excitation test to obtain their mechanical properties according to ASTM E 1876–99 [58]. Resonant Frequency Analyzer (RFA) by IMCE, Belgium was used to measure Young's modulus of all coating samples with the nominal size of 50 mm × 10 mm × 2 mm. To validate the results, the Impulse Excitation test was performed on at least three specimens from each coating samples.

5.7. Three Point Bending Test

There are several good reasons why the three-point-bend test is used extensively in material characterization: economy, simplicity of specimen preparation and testing, ease of adaptability to environmental testing, and the availability of well documented simple formulas for analyzing materials having equal tension and compression properties [59]. Another important reason is that the three-point-bend test is a simple way to subject a specimen to tension, compression, and shear simultaneously. In this sense, a three-point-bend test provides a direct measure of the structural integrity of the material. The bending test configuration setup is shown as Figure 11.

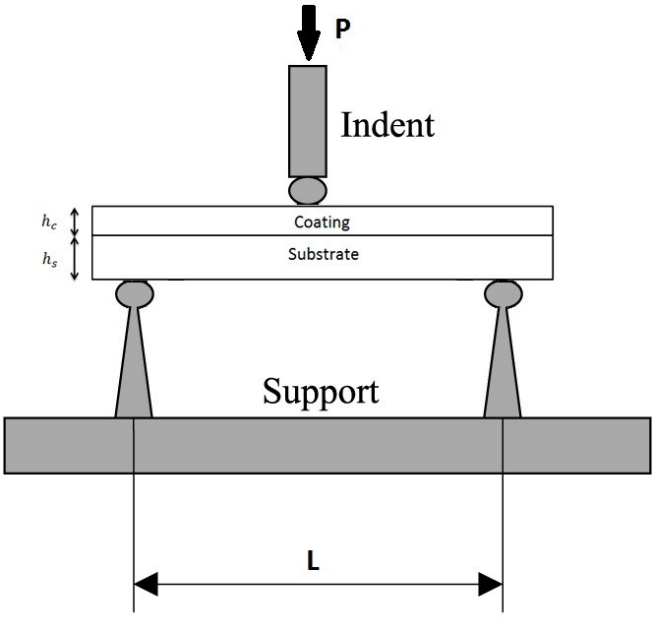

Figure 11. A schematic of a three-point bending test set-up.

The aim of this work was determine the elastic modulus of the coating with and without attached substrate. After the thermal deposition the samples were machined and cut to 13 mm ×60 mm ×2 mm dimensions. This size was chosen from literature; in one similar study they have noticed for capturing more accurate elastic modulus from coating samples with higher porosity a larger ratio of width to thickness is required. In the next section the spin length was determined regarding to ASTM D790 [60]. Since, the coating thickness is not uniform along the width of the samples; the average thickness of the coating was used for calculations. A screw driven testing machine (Instron 5567) was used for three point bending test at a rate of 0.12 mm/min.

CHAPTER 6. RESULTS AND DISCUSSION

6.1. Analytical Model

In this study Hashin-Shtrikman [8] equations were applied to calculate the elastic modulus of Al-Cu cold sprayed composites. This model is specifically developed to predict the elastic modulus of particle-reinforced composites. The equations are expressed as follows:

$$K^{Upper} = K_R + (1-f)\left[\frac{1}{K_M - K_R} + \frac{3f}{3K_R + 4\mu_R}\right]^{-1} \tag{22}$$

$$K^{Lower} = K_M + f\left[\frac{1}{K_R - K_M} + \frac{3(1-f)}{3K_M + 4\mu_M}\right]^{-1} \tag{23}$$

$$\mu^{Upper} = \mu_R + (1-f)\left[\frac{1}{\mu_M - \mu_R} + \frac{6f(K_R + 2\mu_R)}{5\mu_R(3K_R + 4\mu_R)}\right]^{-1} \tag{24}$$

$$\mu^{Upper} = \mu_R + f\left[\frac{1}{\mu_R - \mu_M} + \frac{6(1-f)(K_M + 2\mu_M)}{5\mu_M(3K_M + 4\mu_M)}\right]^{-1} \tag{25}$$

$$E_c = \frac{9K}{1 + 3K/\mu} \tag{26}$$

where K is the Bulk Moduli; μ is the shear moduli; f is the volume fraction of reinforcement. The superscripts ″ Upper ″, ″Lower″, ″M ″ and ″R″ refer to the upper and lower bound estimates, and matrix and reinforcement phases. The estimated E_c values using Hashin-

Shtrikman equation were 74.72 and 86.23 GPa for cold sprayed Al with 10 and 20 vol.% Cu, respectively.

The elastic modulus of wire arc sprayed Alloy 625 coating was calculated using Hashin-Hasselman equation. This is the most commonly applied model for estimating the modulus of porous materials [61]. The average elastic modulus was obtained from three different images which were taken from randomly selected positions along the polished cross-section of the coating. The Hashin-Hasselman equation is defined as follows:

$$E^* = E_0\left[1 + \frac{Ap}{1-(A+1)p}\right] \tag{27}$$

where A is a constant equal to -33.2, E_0 is the elastic modulus of the bulk material, p is the volume fraction of all voids, cracks, and splat interfaces. The elastic modulus (E_0) for the as-sprayed Alloy 625 is 205 GPa and p is equal to 0.024±0.0127. By substituting the above values in Hashin-Hasselman equation, the estimated elastic modulus of the coating (E^*) was to be found 116.52±25.3 GPa.

6.2. Microstructural Characterization

The quality of the cold sprayed composites highly depends on the characteristics of the feedstock powder. Therefore, an important consideration in establishing the spray-microstructure relationship of any deposition process is to understand the characteristics of the feedstock powder. The chemical composition, size distribution, and existence of impurities may directly affect the microstructure of the deposition. A SEM micrograph of both powder blends as feedstock in this study is shown in Figure 12. Two different contrasts in this picture are

associated with aluminum and copper as it is confirmed by EDS measurements of the light and dark regions in these Figures. Average compositions based on measurements from 8 to 10 different spots in these regions, selected from different images, resulted in 98.8±0.5 Al in dark regions and 97.9±0.8 Cu in light regions. These results are in good agreement with the nominal composition provided by powder manufacturer previously reported in section 2.1.

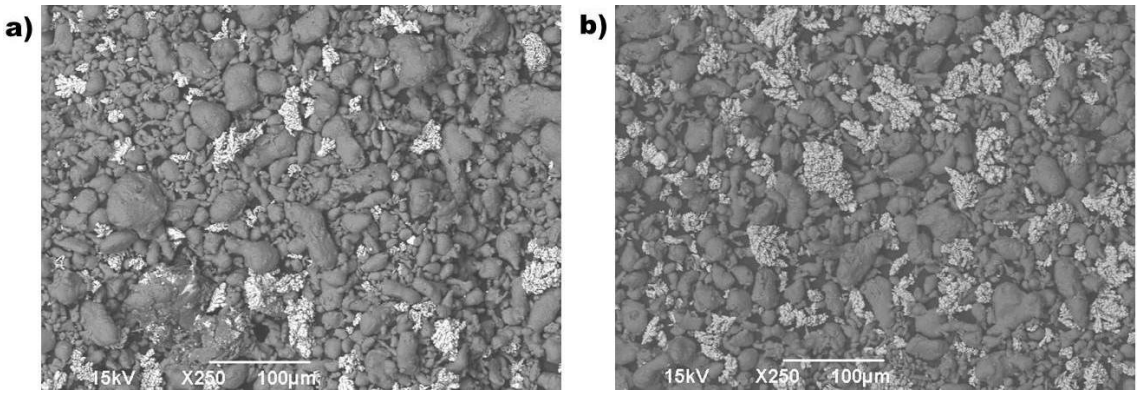

Figure 12. Morphology of feedstock powders used in this study taken by SEM, (a) Al-10% Cu and, (b) Al-20% Cu.

Optical micrographs of a cross-section of cold sprayed composites are shown in Figure 13 (a) un-etched Al-10%Cu and (b) etched Al-10%Cu. The polished cross sections illustrate that the solid particles have deformed and flattened upon impact and there is normally good bonding between the single particles. The coatings are fairly dense with almost no visible pores and voids. The image analysis measurement resulted in less than 1 Area. % of voids and pores within microstructure of both composites as indicated in Table 9. The etched microstructure shows grain boundary within aluminum matrix as shown in Figure 13 (b).

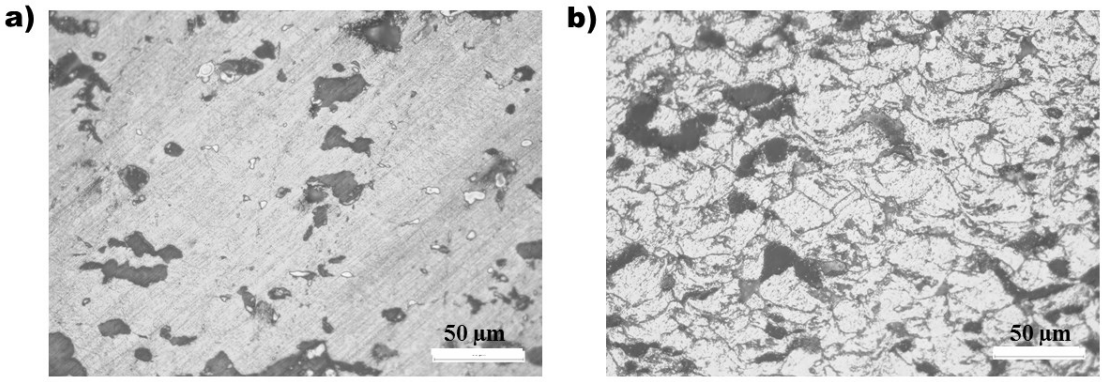

Figure 13. Optical micrographs from (a) un-etched Al-10% Cu and,
(b) etched Al-10% Cu samples.

Backscattered electron SEM images of un-etched cross-sections of cold sprayed composites are shown in Figure 14 (a) Al-10%Cu and (b) Al-20%Cu. There is no splat boundary visible in these images indicating very good cohesion between impacted particles. Areas of three discernible levels of contrast, black, gray, and white, are seen in these SEM micrographs. The round shape black regions within the gray area are identified as pores. Additional characterization by EDS was conducted to determine the composition of the gray and white area in both images. EDS results indicate that the gray regions are aluminum matrix and white regions are copper.

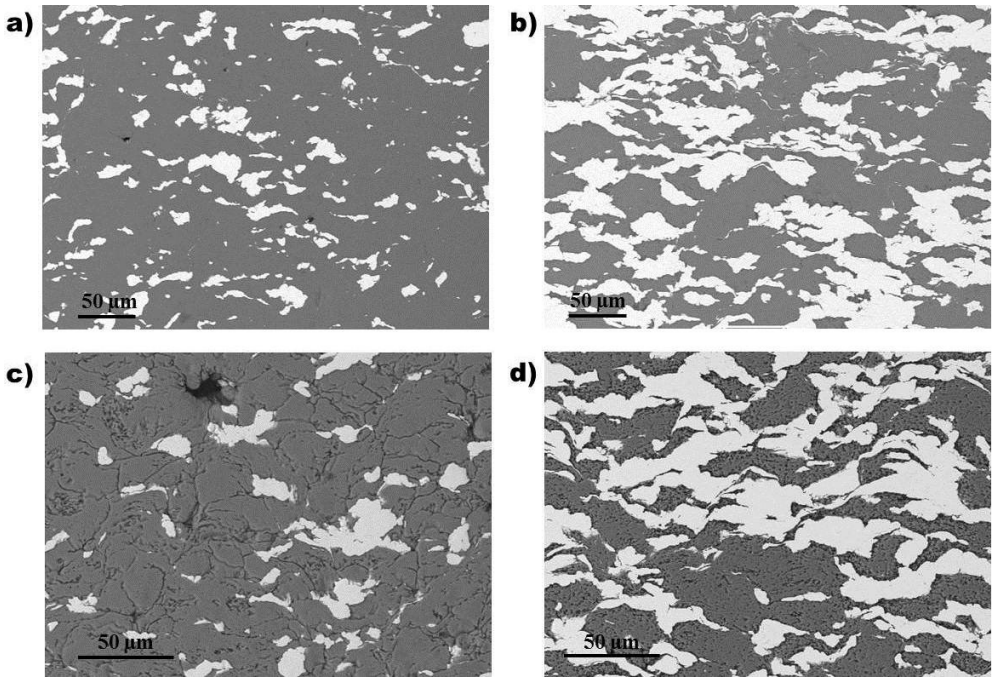

Figure 14. SEM image of cross-section of cold sprayed (a) un-etched, and (c) etched Al-10% Cu, (b) un-etched, and (d) etched Al-20% Cu.

Although, only 10% and 20% copper particles by volume were added to the aluminum matrix, the visible area percentage of the copper seems to be more within the microstructure of the two different composites. Table 9 lists the average area percentage of each contrast obtained by from image analysis on several micrographs. It is worth mentioning that the higher apparent area percentage of copper within the microstructure is due to the larger particle size of the copper powders as shown in the above figure (Figure 14). It can also be associated with higher deformation rate of aluminum particles during the impact which resulted in more flattening and spreading of the white regions within the microstructure. The values shown in Table 9 is for area percentage measurement whereas, the actual volume percentages of copper particles in feedstock are 10 and 20 for the deposited composites.

Table 9. Measured area percentage of each contrast within the microstructure of composites using image analysis.

Area %. / Sample	Al	Cu	Voids
$E_{Al\text{-}10\%\ Cu}$	87±1	12.25±0.55	0.75
$E_{Al\text{-}20\%\ Cu}$	58.75±0.8	40.25±1	1±0.35

The SEM image of cross-section of Alloy 625 is shown in Figure 15. Areas of three discernible levels of contrast, black, gray, and dark gray are seen in these SEM micrographs. The round shape black regions within the gray area are identified as pores. The polished cross sections illustrate a considerable area of oxidation along the splat boundaries (dark grey region). The coatings are fairly dense with some pores and voids. Table 10 lists the average area percentage of each contrast obtained by from image analysis on several micrographs. The image analysis measurement resulted in a 27 and 2.4 Area % of oxidation and voids, respectively, within microstructure of Alloy 625 wire arc coating.

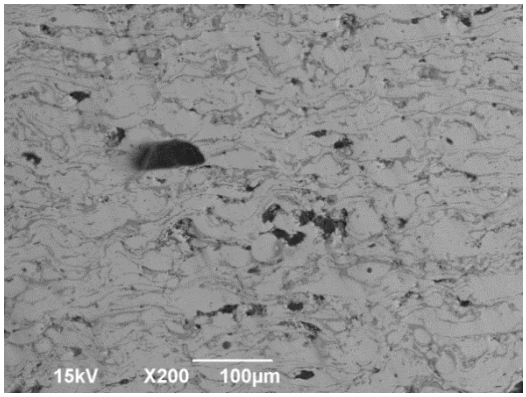

Figure 15. SEM image of cross-section of Alloy 625 wire arc spray coating.

Table 10. Measured area percentage of each contrast within the microstructure of coating

Area %. / Sample	Alloy625	Cr_2O_3	Voids
$E_{Alloy625}$	70.6±12	27±7	2.4±1

6.3. Mechanical Testing

6.3.1. Knoop Hardness

Figure 16 shows the Optical micrograph of the Knoop indentation made on the Al-20 Vol.% Cu sample. There are no visible cracks in the region of the matrix and matrix/particle interface, which indicates high ductility of the composite after cold spraying.

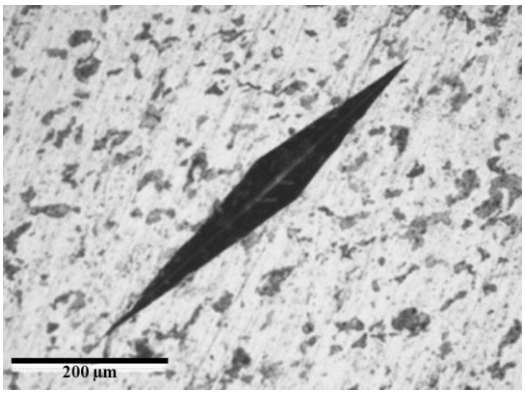

Figure 16. Optical micrograph showing indentations made on the region containing Al matrix and Cu particles for the composite reinforced with 20% Cu by volume.

A schematic of the microstructure of a coating defining directions of the Knoop indentations parallel and perpendicular to the coating plane is shown in Figure 17.

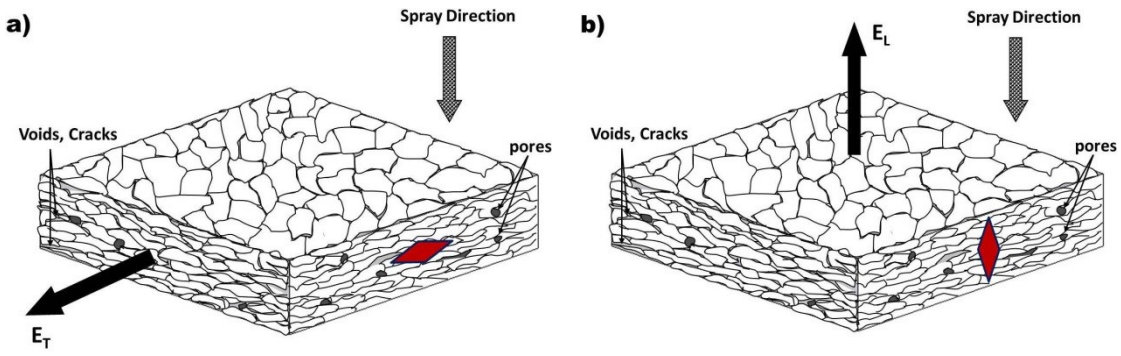

Figure 17. (a) Knoop indentation in transverse direction (b) Knoop indentation in longitudinal direction.

Figure 18 indicates the change in the measured hardness value along with the correspondent elastic modulus for each indentation measurement in both transverse and longitudinal direction of Al-10% Cu by volume. The calculated elastic modulus using the Knoop hardness measurement in transverse and longitudinal direction for Al-20% Cu by volume is shown in Figure 19.

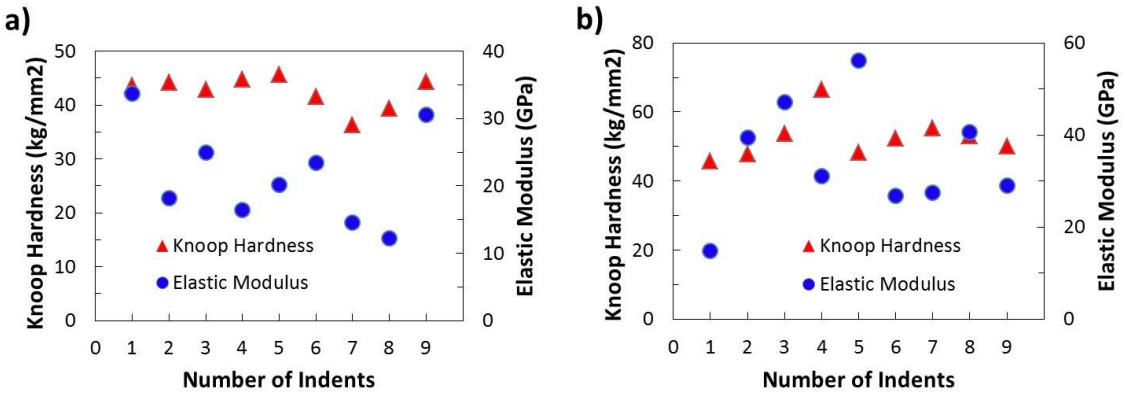

Figure 18. Knoop hardness value and calculated elastic modulus for each indentation measurement of Al- 10% Cu in: (a) transverse direction, and (b) longitudinal direction.

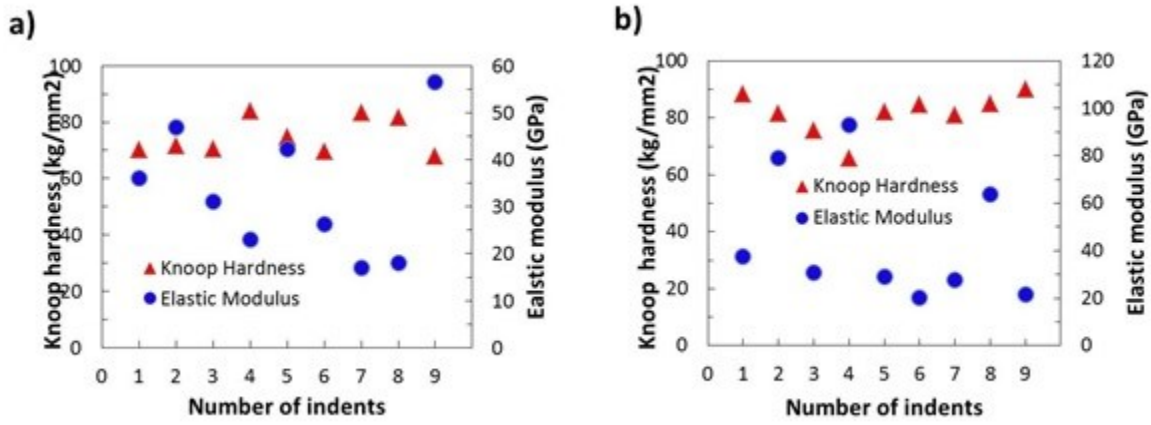

Figure 19. Knoop hardness value and calculated elastic modulus for each indentation measurement of Al- 20% Cu in: (a) transverse direction, and (b) longitudinal direction.

The complete results of the Knoop experiments and correspondent elastic modulus of the both cold sprayed composite samples in both transverse and longitudinal directions are tabulated

in Table 11. The changes in the value of elastic modulus are not significant instead of higher measured values for hardness in Al - 20% Cu by volume which is due to the smaller b'. However, the calculated values are significantly lower than the ones measured from analytical methods.

Table 11. Microhardness and elastic modulus obtained from Knoop hardness test.

Specimen	Hardness (HKN)*	Elastic Modulus (GPa)*
Al-10% Vol. Cu (Transverse)	42.5±3	21.6±2
Al-10% Vol. Cu (Longitudinal)	52.6±6	34.7±9
Al-20% Vol. Cu (Transverse)	74.8±5	33±10
Al-20% Vol. Cu (Longitudinal)	82.9±4	46.2±13

*Average of 9measurements ±1 standard deviation for Al-Cu.

Figure 20 is a plot of the indentation versus Knoop hardness and elastic modulus in both the transverse and longitudinal directions of Alloy 625. The Knoop hardness in the longitudinal and transverse directions are 318.50±21.75 and 299.71±18.55 HKN, respectively. After statistical outliers being discarded, from 13 tests the corresponding average modulus in the longitudinal and transverse directions were calculated 51.23±8.24 and 70.14±17.43, respectively. The obtained elastic modulus from the Marshall equation is directly related to the indentation width after fully elastic-recovery. Since in anisotropic materials the elastic-recovery of the indentation width can vary independently from the indentation length and the fact that the Knoop hardness equation is only related to the length of the indentation, higher Knoop hardness value may not result in higher elastic modulus.

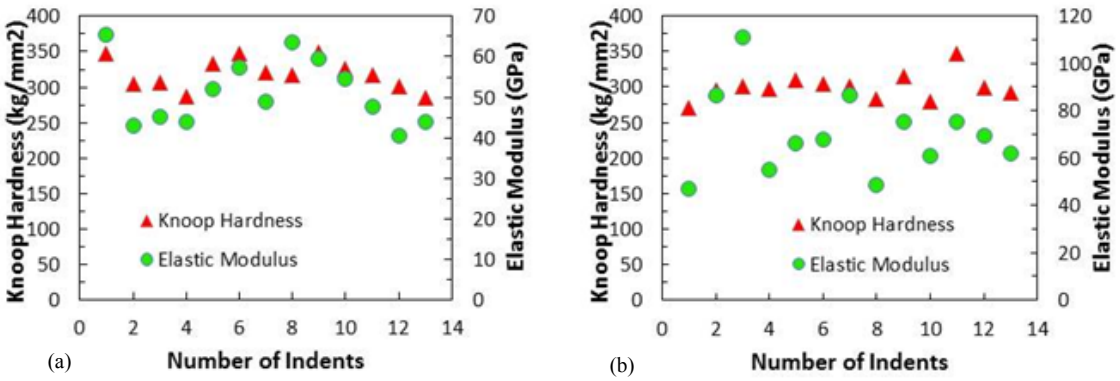

Figure 20. Knoop indentation plots in (a) longitudinal and (b) transverse direction

The complete results of the Knoop experiments and correspondent elastic modulus of the Alloy 625 samples in both transverse and longitudinal directions are tabulated in Table 12. The changes in the value of elastic modulus are not significant instead of higher measured values for hardness in Al - 20% Cu by volume which is due to the smaller b'. However, the calculated values are significantly lower than the ones measured from analytical methods. The large scattering in hardness values and consequently large variation in calculated elastic modulus could be due to heterogeneous microstructure of coating materials for both samples. The variations in hardness value are resulted from different phases existing in the microstructure. For instance the higher elastic modulus might be a related to an oxide region in the microstructure.

Table 12. Microhardness and elastic modulus obtained from Knoop hardness test.

Specimen	Hardness (HKN)*	Elastic Modulus (GPa)*
Alloy 625 (Transverse)	299.71±18.55	70.14±17.43
Alloy 625 (Longitudinal)	318.50±21.75	51.23±8.24

*Average of 13 measurements ±1 standard deviation for Alloy 625 samples.

6.3.2. Nano Indentation

Nano indentation test was only performed on Alloy 625 samples. Two series of tests were performed by nanoindentation on Alloy 625 wire arc spray coating. The first test consisted of identifying oxide and non-oxide regions to determine the mechanical properties difference between the two regions. The second test averaged both oxide and a non-oxide region so that total average of mechanical properties for Alloy 625 could be reported, through 100 equally spaced indents. For the first test, three indents were done on non-oxide regions of Alloy 625 and six indents were performed on the oxide regions. Assuming a Poisson ratio of 0.31 for Alloy 625 [14], the average modulus of elasticity for the non-oxide regions was 188.25±32.9 GPa and the average indentation hardness was 6.49±0.24 GPa. For the oxide region, the average modulus of elasticity was 217.04±22.54 GPa and the average indentation hardness was 7.58±1 GPa. Figure 21 and Figure 22 show the load-displacement curves for the non-oxide and oxide regions respectively. Depth of penetration varied between 100 and 200 nm. The oxide regions had higher elastic modulus and hardness, however the challenge of adequately identifying oxides lead to larger standard deviations. It is believed that more indents can improve statistical results.

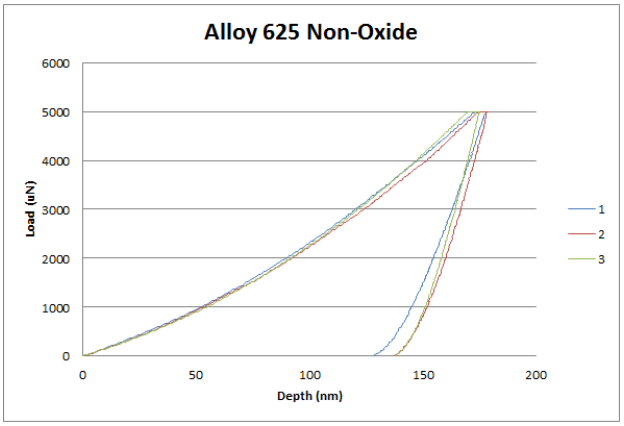

Figure 21. Load-displacement curves for non-oxide regions of Alloy 625

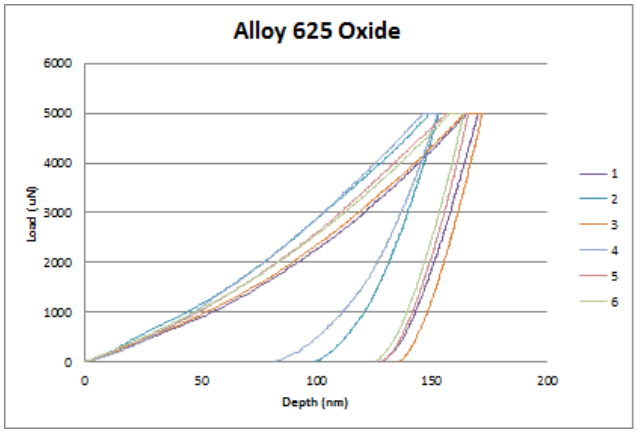

Figure 22. Load-displacement curves for oxide regions of Alloy 625

The second test averaged 100 indents in a line spaced 10 μm apart randomly selecting oxide and non-oxide regions. The average modulus of elasticity for Alloy 625 was 211.13± 29.89 GPa and the indentation hardness was 7.85± 3.12 GPa. The values determined from these set of tests are in a good agreement with the reported values in the literature. The results from these tests have been implemented in the numerical simulation for determining the elastic modulus of Alloy 625.

6.3.3. Resonance Frequency Test

The Impulse Excitation test was performed on at least three specimens from each composition and the average Young's modulus was 31.31±1.02 GPa and 46.48±2.61 GPa for 10% and 20% copper by volume, respectively. According to the resonance frequency test on the Alloy 625 test specimens the elastic modulus was to be found 57.41±1.47 GPa in longitudinal directions. Also the Poisson's ratio of Alloy 625 coating deposited by wire arc spray method was determined to be 0.275 using the same test. These results are accurate and can be used as

reference to compare the accuracy of the results from the other experimental, analytical, and numerical techniques. These results are in good agreement with the ones obtained from Knoop indentation test.

The experimental results from different mechanical testing to determine elastic modulus of cold sprayed Al-Cu composite in this study are in good agreement. However, it is important to compare these results with the ones reported for the same material manufactured by a conventional process. The comparison of the results will show the effectiveness of cold spraying in production of metal matrix composites. Torralba, et al studied on Al-Cu matrix composites by squeeze casting (SC) and determined a modulus of 70.5 GPa for this material. The composition was not explicitly stated in their report however, from image analysis of provided images in their report a 20% Cu composition was determined. The modulus calculated from Knoop indentation of the cold spray samples in this study is 34% less than that of the squeeze casting samples [62]. Generally, Squeeze casting fabricated components exhibit fine grain microstructure with significantly improved properties over other conventional methods. SC process consists of melting and solidification of materials inside a re-usable die under high pressure condition. [63]. However, It seems that cold spraying is a faster technique with less time required for sample preparation. In addition, SC molded parts also requires production of dies for casting which wear overtime. The mechanical properties of cold spraying can be improved upon application of an appropriate post deposition heat treatment.

6.3.4. Tensile and Bend Test

Figure 23 (a) shows example of alloy625 tensile sample after testing. As shown the tests were ended after sample's fracture. In Figure 23 (b) three-point bend testing has been conducted on an alloy625 coating sample.

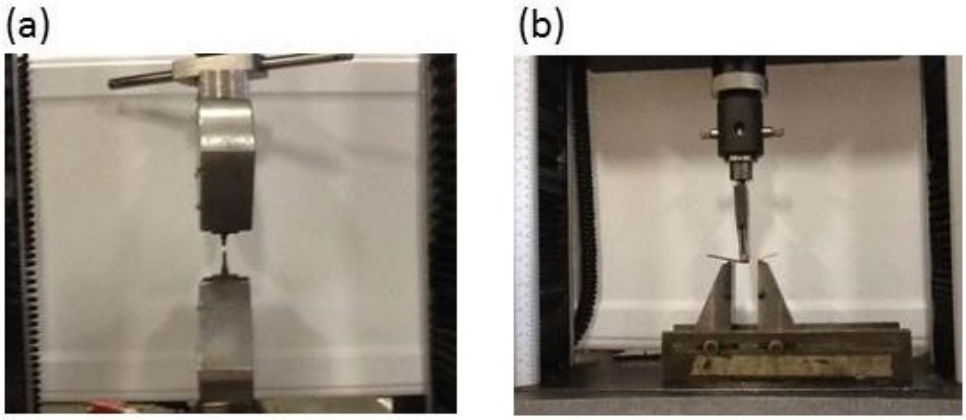

Figure 23. (a) Alloy 625 samples after tensile test (b) an image of bend test on alloy625 sample.

A typical stress-strain curve for Alloy 625 wire arc spray coating measured from the tensile test is shown in Figure 24 (a). Five tensile tests were completed, the average elastic modulus was 18.98 ±3.08 GPa. The elastic modulus calculated in the tensile test was in the transverse direction. The three point bend test was completed on substrate and coating from which the elastic modulus of the Alloy 625 wire arc spray coating was found to be 65.74±12.41 GPa. The bend test provides the modulus in the longitudinal direction. A standard loading (load-displacement) diagram is shown in Figure 24 (b) for the three-point bend test.

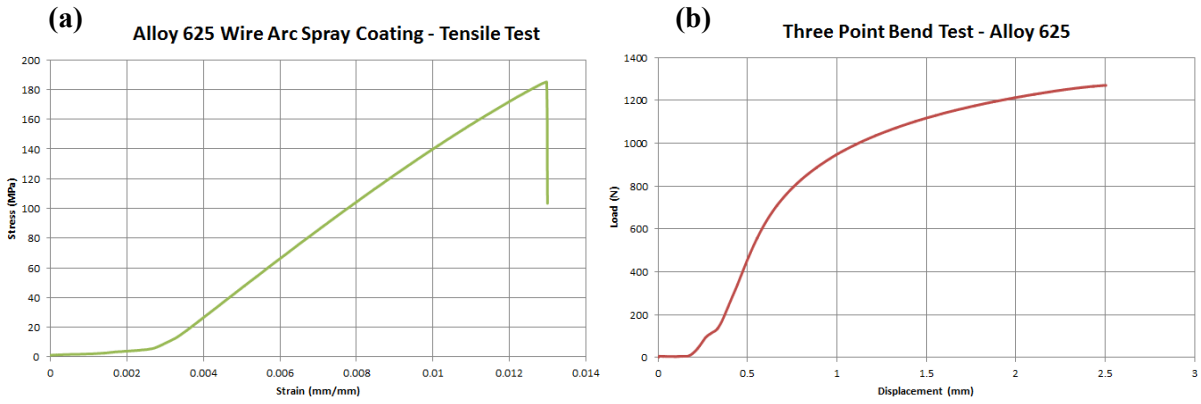

Figure 24. (a) A typical stress-strain curve from the tensile test for Alloy 625 wire arc sprayed coating. (b) typical Loading curve for the three point bend test.

The elastic modulus obtained from tensile test was significantly lower than that of the Knoop - technique. This could be partly due to the small sample sizes and voids present which can significantly affect the accuracy of the tensile test. As seen from stress-strain curve from the tensile test in Figure 24 (a), the coating is brittle with no plastic deformation. The measured elastic modulus results from the bending test were in relatively good agreement with resonant frequency and Knoop values.

6.4. Numerical Simulation

There are several commercially available finite element packages which are capable of numerical simulation of stress-strain distribution and mechanical behavior of the bulk and homogenous structures. Mechanical characteristics of inhomogeneous materials such as coating structures highly depend on their microstructural features such as porosity, voids, and interface between splats and it is essential to account for these features in finite element models of coating behavior. The Object Oriented Finite element program(OOF), developed by US National

Institute of Standards and Technology (NIST), uses actual micrographs to numerically simulate thermo-mechanical properties of coatings and composite materials [64].

Several microstructural images were taken from randomly selected positions along the polished cross-section of the cold sprayed Al-cu coatings. The image files were converted to portable pixel map format (ppm) from their original formats (i.e. jpeg, TIFF, etc.). The portable pixel map (ppm) incorporates microstructural data with basic material data (such as Poisson ratio and elastic modulus), and materials physical models in the form of experimental or simulated micrographs [63]. By setting a threshold level for the pixel brightness, the pixels were divided into three groups, matrix (gray), reinforcement phase (white), and voids (black). The threshold value must be set up appropriately in order to select the most pixels with same contrast as one representative material [14,64,65]. In this study several threshold value iterations as discussed in [14] have been used in order to determine the optimum threshold value for pixel selection process. Figure 25 (a) illustrates an image consisting of matrix, reinforcement particles, and voids within microstructure of Al-Cu coating. The selected area is meshed and divided to several elements. Some of those elements may contain pixels corresponding to mixture of different phases. The pixel selection and mesh geometry must be improved to increase the accuracy of the solution. Figure 25 (b) shows the red selected meshes with homogeneity index of lower than 80%. The higher homogeneity index would result in more accurate results. In this simulation the homogeneity index varies from 84%-88% for different SEM micrographs. Due to the ambiguity in recognizing boundaries between different material's pixels in the micrograph; as shown in Figure 25 (c) and (d) the meshes need to be refined and annealed several times. This process would cause in higher homogeneity index, and higher computational time, as well. The

homogeneity index is defined as the ratio of the area of the dominant category to the area of the element as a whole.

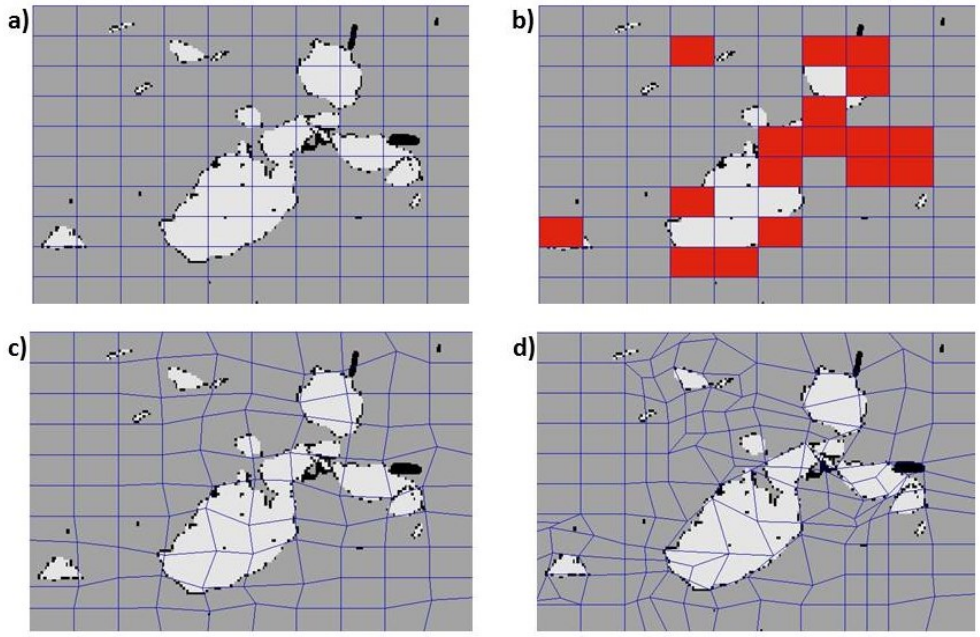

Figure 25. An SEM micrograph from a cross-section of cold sprayed Al-10% Cu by volume (a) meshed with n_x=110 and, n_y=125 size, (b) binary image illustrating meshes with a homogeneity index lower than 80%, (c) after 15 iteration of annealing, (d) after 1 iteration of refining and adapting.

Figure 26 (a) shows an original SEM micrograph of the cross-section of the as-sprayed coating. Microstructural features could then be grouped according to their colors and threshold level of pixel brightness (contrast). Each group was named and material properties such as Elastic modulus, E, and Poisson ratio, υ, were assigned to each group and all the pixels in the individual group. It produced a grayscale (binary) image as shown in Figure 26 (b). Then, the binary image was meshed by dividing it to thousands of individual elements. A quadrilateral element with a second polynomial order was adapted as meshes. The meshed image as shown in Figure 26 (c) is used for computation of mechanical properties.

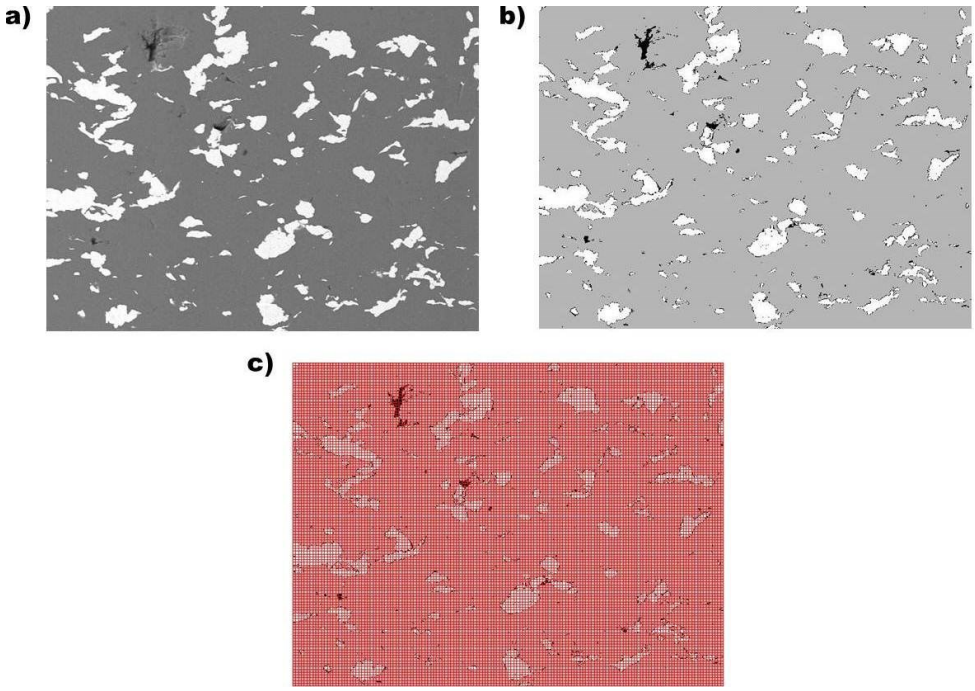

Figure 26. (a) An SEM micrograph from a cross-section of cold sprayed Al-10% Cu by volume, (b) processed binary image, (c) meshed image.

A uniaxial strain corresponding to the strain below the yield strength of bulk aluminum was imposed to the cross-section parallel and perpendicular to the coating plane (the transverse and longitudinal directions). Five images taken from different regions within the cross-section of each coating sample have been analyzed to reduce the dependence of the results on the location of the image within the microstructure. The estimated elastic modulus for Al-10% Cu by volume in transverse and longitudinal directions using finite element were 86.5±3 GPa and 95.3±6 GPa, respectively. The estimated elastic modulus for Al-20%Cu in transverse and longitudinal directions using finite element were 97.2±6 GPa and 106.7±11 GPa, respectively. from the results obtained in longitudinal direction are not accurate since elastic modulus of each constituents is less than 100 GPa and calculated elastic modulus above 100 GPa will not be acceptable. Therefore, the results from application of image based finite element in longitudinal

direction have not been included in this study. Figure 27 (a) and (b) exhibit stress distribution in the micrograph shown in Figure 26, after application of load in the transverse and longitudinal directions.

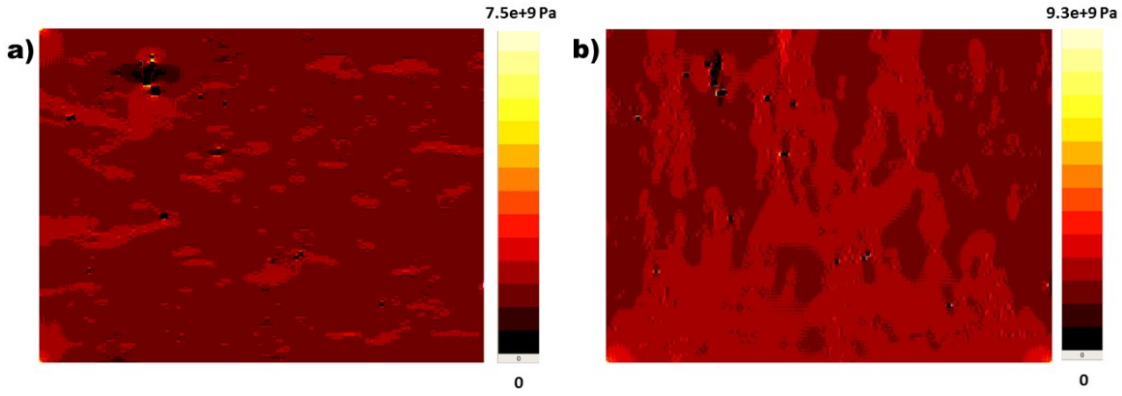

Figure 27. Stress distribution in micrograph shown in Figure 26 after application of loads in: (a) transverse and (b) longitudinal directions.

The elastic modulus of composite in longitudinal direction for Al-10% Cu was found to be greater than that for transverse one using object oriented finite element analysis. This is against what has already been reported for coating materials since the weak splat boundaries will reduce the mechanical strength and elastic modulus [66]. It can be explained by observing at high magnification microstructural images such as the ones shown in Figure 14. No visible splat boundary can be seen in the microstructure of cold sprayed samples due to high impact velocity and strong bounding between splats. The distribution, orientation, and shape factor (lower aspect ratio) of the stronger phase Cu particle might be another reason for exhibiting better mechanical properties in longitudinal direction. Elastic modulus calculation in image based finite element highly depends on the amount and distribution of each contrast within the image. According to Table 9 the visible area percentage of copper as stiffer material is much higher than the actual volume percentage of the reinforcement phase used in feedstock. It can be another reason of significantly larger calculated elastic modulus by numerical simulation compare to experimental

results. The Numerical simulation also uses 2D images to calculate 3D properties such as elastic modulus. Experimental results are consistent and close while analytical calculation resulted in larger calculated elastic modulus in coatings. This discrepancy between the analytical calculations and experimental values of elastic modulus are due to the failure of the analytical models to account for the effect of the features such as voids and pores across the microstructure.

The image based finite element analysis was also conducted on wire arc sprayed Alloy 625 coating samples. Figure 28 (a) shows an original SEM micrograph of the cross-section of the as-sprayed coating. Next, microstructural features were identified and grouped based on their pixel colors and brightness threshold level (contrast). Each phase was assigned an elastic modulus and Poisson's ratio for all the pixels in the phase cluster forming a "material image" as shown in Figure 28 (b). In the next step, thousands of individual meshes were generated on the material image. Each element may contain pixels corresponding to multiple phase regions. As shown in Figure 28 (c) quadrilateral elements with second order polynomial was adapted to mesh the material image. Finally, the loads were applied to the meshed image and the mechanical properties were obtained.

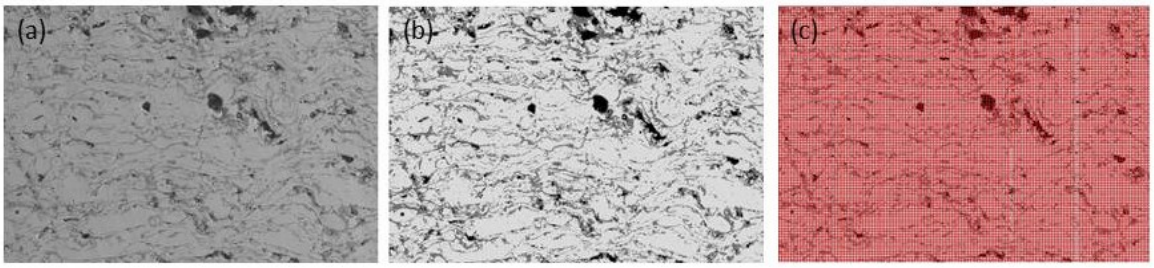

Figure 28. (a) An SEM micrograph from a cross-section of wire arc sprayed Alloy 625, (b) processed material (binary) image, (c) meshed image.

For the remaining elastic region, the uniaxial corresponding strain was selected below the yield strength of bulk nickel. Loads were applied to the coating cross-section in both the transverse and longitudinal directions. Due to the variation in the phase distribution of different microstructure images, five images taken from different regions within the cross-section of each coating sample have been simulated to reduce the dependence of the results on the location of the image within the microstructure. The estimated elastic modulus for Alloy 625 in transverse and longitudinal directions using finite element were 174±8 GPa and 148±32 GPa, respectively. The elastic modulus of each phase was defined through nanoindentation test. Figure 29 (a) and (b) shows the stress distribution in the microstructure image, after application of load in the transverse and longitudinal directions, respectively.

Alternatively, the elastic modulus for each phase was defined from literature review [6]. The estimated elastic modulus under these properties in transverse and longitudinal directions through numerical simulation was 214.4±13 GPa and 189.8±45 GPa, respectively. The simulations which were run with nano-indentation obtained Young's modulus shows a slightly lower overall elastic modulus and closer to experimentally obtained results.

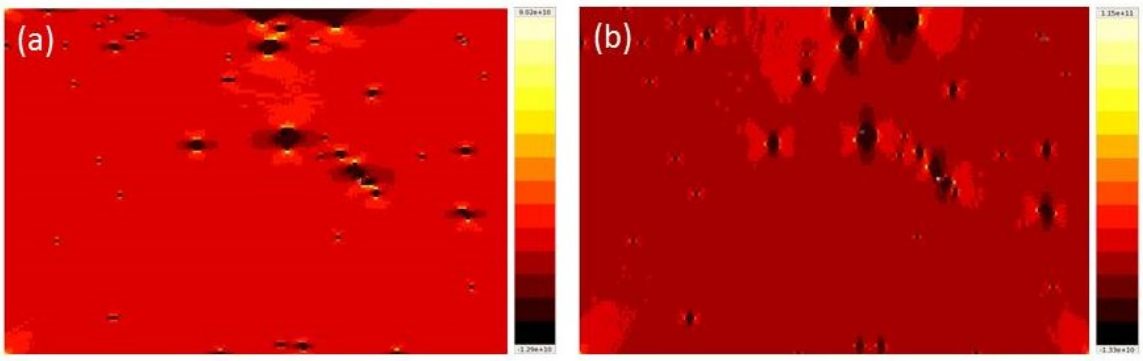

Figure 29. Stress distribution in micrograph after application of loads in: (a) transverse and (b) longitudinal directions.

OOF analysis consistently predicted the elastic modulus of Alloy 625 coating in the transverse direction to be greater than the longitudinal regardless of phase distribution. The distribution, orientation, and geometry of the splat boundaries may contribute to better mechanical properties in the transverse direction.

One of the purposes of utilization of image based finite element in this study was to investigate the effectiveness of such methods in accurate evaluation of mechanical properties of thermally sprayed coatings. The image based finite element study was unable to address the effect of important parameters such as presence of unwanted phases, interfacial properties between splats, and loading conditions.

6.5. Comparison of the Results

In this section the results from different methods for Al-Cu has been tabulated as Table 13 and Alloy 625 wire arc spray coating as Table 14.

Table 13. Elastic modulus results for Al-Cu samples in transverse and longitudinal directions.

Method	Material	$E_{transverse}$(GPa)	$E_{Longitudinal}$(GPa)
Theoretical (Hashin-Shtrikman Hashin-Hasselman)	$E_{Al-10\%Cu}$	74.72	74.72
	$E_{Al-20\%Cu}$	79.64	79.64
Experimental (Resonance Frequency)	$E_{Al-10\%Cu}$	----	31.3 ± 1.02
	$E_{Al-20\%Cu}$	----	46.48 ± 2.68
Experimental (Indentation Test)	$E_{Al-10\%Cu}$	21.6±2	34.7±9
	$E_{Al-20\%Cu}$	33±10	46.2±13
Finite Element Analysis (OOF)	$E_{Al-10\%Cu}$	84±3	95.3±6
	$E_{Al-20\%Cu}$	97.2±6	106±11

Table 14. Elastic modulus results for Alloy 625 sample in transverse and longitudinal directions.

Method	$E_{transverse}$	$E_{Longitudinal}$
Theoretical (Hashin-Shtrikman Hashin-Hasselman)	116.52±25.3	116.52±25.3
Experimental (Resonance Frequency)	----	57.41±1.47
Experimental (Indentation Test)	70.14±17.43	51.23±8.24
Experimental (Tensile Test)	18.98±1.23	----
Experimental (3 Point Test)	65.74±12.41	----
Finite Element Analysis(OOF)	174±8 GPa	148±32

CHAPTER 7. CONCLUSION AND FUTURE WORKS

This study examined microstructural-based mechanical properties of a cold sprayed aluminum containing different volume percentage of copper particulate reinforcement, and wire arc sprayed Alloy 625 coating. Cold spraying technique was used to fabricate composite samples instead of traditional fabrication routes such as casting or powder metallurgy. Cold spraying is a rapid technique to fabricate metal matrix composites in a single step. The composite material consisted Al matrix reinforced with 10 and 20 vol.% of Cu particulates. Wire arc spraying technique was used to deposit Alloy 625 coating on an Alloy 625 substrate. Wire arc technique is a highly thermal efficient, relatively inexpensive, and rapid method capable of fabricating metal matrix composites in a single step and can be used as a coating mechanism for superalloys.

Several experimental, numerical and analytical methods were performed on the Al-Cu cold spray and wire arc Alloy 625 composites. It is essential in coating layers design and processes to compare all those results to predict the elastic modulus of metal matrix composites in both transverse and longitudinal directions. The comparison of the analytical and numerical results with actual values obtained from experimental techniques indicated the effectiveness of each technique to evaluate mechanical properties of deposited composite materials. Furthermore, nanoindentation test was performed on Alloy 625 coating, to better address the mechanical properties of oxide and non-oxide regions of the microstructure. These results were also used in the numerical simulation to calculate the elastic modulus of the Alloy 625 micro-schemes.

The elastic modulus obtained from the theoretical models for Al-Cu and Alloy 625 composites was higher than actual results obtained from experimental tests. It can be resulted from the inaccuracy and inability of the models to capture all microstructural features which define mechanical properties of deposited composites. There was a significant difference

between the values of the elastic modulus obtained from image based finite element and the ones measured experimentally. The predicted values by numerical simulation were closer the ones obtained from analytical models and much higher than the actual values measured experimentally. In the Al-Cu cold spray coating case, it can be attributed to the large area percentage of the copper with higher elastic modulus within the micrographs and no visible splat boundary within the coating microstructures. Furthermore, for both composite materials the interfacial properties between splats are not taken to account in the numerical simulation models and therefore are a potential source of error in the obtained elastic modulus. In addition, the image based finite element is a 2D technique but elastic modulus is a 3D characteristic of a material. This study showed that image based numerical simulation was inaccurate and far from the obtained experimental results. It is due to inability of taking to the account the interfacial properties of the coatings to the inputs for more accurate simulations for the mechanical characteristics of the coating materials.

The results obtained from application of available analytical models such as Hashin-Shtrikman and Hashin-Hasselman resulted in higher values compared to the experimental results. It could be due to the fact that those analytical models are unable to include interfacial properties and splat boundary areas into the calculations. This missing information would result in an overestimation for the elastic modulus of studied materials. However the obtained results from the analytical methods were in better agreement with the experimental results compared to the the ones obtained from numerical simulations.

Overall results from the experimental tests are in relatively good agreement for Al 10 and 20% of Cu by copper composites and Alloy 625. The Knoop test and resonant frequency methods produced the most consistent results. With thin coatings the Knoop and bend tests have an added benefit of not requiring coating separation from substrate which can be a difficult task. Examination and comparison of the results are strong indications of the influence of the microstructure characteristics on the mechanical properties of thermally spray deposited metal matrix coatings. In closing, interfacial properties were found to be immensely important and continue to be an area of future research.

7.1. Future Research

The group is planning on developing an empirical model which elucidates the relationship between the physical and mechanical properties and microstructure of coatings. This model will be independent of the coating materials and production technique. This would require an in depth understanding of the effect of interfacial properties on the overall mechanical properties of coating materials.

REFERENCES

1. C.C. Brendt, W. J. Lenling, Handbook of Thermal Spray Technology, in: J.R. Davis (Ed.), Cold Spray Process, ASM International., Ohio, 2004.
2. Michlik P., and Berndt C., Image based extended finite element modeling of thermal barrier coatings. Surface & Coating Technology, 2006; 201: 2369-280.
3. Nakamura T., Qian G., and Berndt C. C., Effects of Mechanical properties of plasma-sprayed ceramic coatings, J. Am. Ceram. Soc. 2000:83-578-584.
4. W. Y. Lee, D. P. Stinton, C. C. Berndt, F. Erdogan, Y-D. Lee, and Z. Mutasim, Concept of Functionally Graded Materials for Advanced Thermal Barrier Coating Applications, Journal of the American Ceramic Society, (1996).
5. R. M. Spriggs, Expression for Effect of Porosity on Elastic Modulus of Polycrystalline Refractory Materials, Particularly Aluminum Oxide, J. Am. Ceram. Soc., 44 (1961) 628-629.
6. C. J. Li, A. Ohmori, and R. McPherson, The Relationship between Microstructure and Young's Modulus of Thermally Sprayed Ceramic Coatings, J. Mater. Sci., 32 (1997) 997-1004.
7. C. J. Li, A. Ohmori, and Y. He, Characterization of Structure of Thermally Sprayed Coatings, 15th ITSC, Thermal Spray: Meeting the Challenges of the 21st century, C. Coddet (Ed.) ASM International, Materials Park, OH, USA, pp. 717-722, (1998).
8. Z. Hashin, S. Shtrikman, A variational approach to the theory of the elastic behaviour of multiphase materials, J. Mech. Phys. Solids., 11 (1963) 127.
9. C.T. Sun, J.L. Chen, G.T. Sha, and W.E. Koop, Mechanical Characterization of SCS-6/Ti-6-4 Metal Matrix Composite, J. Compos. Mater. 24 (1990) 1029-1059.

10. H. Shen, C.J. Lissenden, 3D finite element analysis of particle-reinforced aluminum, Mater. Sci. Eng., A, 338 (2002) 271-281.
11. N. Chawla, R.S. Sidhu, V.V. Ganesh, Three-dimensional visualization and microstructure-based modeling of deformation in particle-reinforced composites, Acta Mater. 54 (2006) 1541-1548.
12. P. Kenesei, A. Borbély, and H. Biermann, Microstructure based three-dimensional finite element modeling of particulate reinforced metal–matrix composites, Mater. Sci. Eng., A, 387–389 (2004) 852–856.
13. N. Chawla, and Y. L. Shen, Mechanical Behavior of Particle Reinforced Metal Matrix Composites, Adv. Eng. Mater. 3 (2001) 357-370.
14. F. Azarmi., T.W. Coyle, and J. Mostaghimi, Young's modulus measurement and study of the relationship between mechanical properties and microstructure of air plasma sprayed Alloy 625, Surf. Coat. Technol. 203 (2009) 1045-1054.
15. T.H. Van Steenkiste, J.R. Smith, R.E. Teets, Aluminum coating via kinetic spray with relatively large powder particles, Surface and Coating Technology 154 (2002) 237-252.
16. D. B. Marshall, Tatsuo Noma, and A. G. Evans, A Simple Method for Determining Elastic Modulus-to-Hardness Ratios using Knoop Indentation Measurements, Communication of the American Ceramic Society, Oct 1982.
17. B. R. Lawn and V. R. Howes, Elastic Recovery at Hardness Indentations, J. Mater. Sci., 16 [10] 2745-52 (1981).
18. Sang-Ha Leigh, Chung-Kwei Lin, and Christopher C. Berndt, Elastic Modulus of Thermal Spray Deposits under Indentation Tests, J. Am. Ceram, Soc., 80 [8] 2093-99 (1997).

19. J. H. You, T. Hoschen, S. Lindig, Determination of Elastic modulus and Residual Stress of Plasma-Sprayed Tungsten Coating on Steel Substrate, Journal of Nuclear Materials, 2006.
20. J. Mencik, Mechanics of Components with Treated or Coated Surfaces, Kluwer Academic Publishers, Dordrecht, 1996.
21. H. Li, K.A. khor, P. Cheang, Young's modulus and fracture toughness determination of high velocity oxy-fuel-sprayed bioceramic coatings, Surfeace and Coatings Technology 155 (2002) 21-32.
22. Hyung-Jun Kim, Young-Gak Kweon, Elastic modulus of plasma-spreayed coatings determined by indentation and bend tests, Thin Solid Films 342 (1999) 201-206.
23. Karlis A. Gross, S. Saber-Samandari, Revealing mechanical properties of a suspension plasma sprayed coating with nanoindentation, Surface & Coating Technology, 203 (2009) 2995-2999.
24. J. P. Singh, M. Sutaria, and M. Ferber, Use of the indentation technique to measure elastic modulus of plasma sprayed zirconia thermal barrier coating, Argonne Technology Division Argonne National Laboratory (1997).
25. R. M. Spriggs, Expression for Effect of Porosity on Elastic Modulus of Polycrystalline Refractory Materials, Particularly Aluminum Oxide, Journal of the American Ceramic Society, 44 (12) (1961) 628-629.
26. Z. Hashin, S. Shtrikman, A variational approach to the theory of the elastic behaviour of multiphase materials, J. Mech. Phys. Solids., 11 (1963) 127.
27. Z. Hashin, J. Appl. Mech-T, ASME 29 (3) (1962) 143-150.

28. Y. H. Zhao, G. P. Tandon, G. J. Weng, Elastic Moduli for a Class of Porous Materials, Acta Mechanica, 76 (1989) 105-130.

29. Y. H. Zhao, G. J. Weng, J. Appl. Mech- T, ASME 57 (1990) 158-167.

30. J. C. Halpin and J. L. Kardos, The Halpin-Tsai Equation: A Review, Polymer Engineering & Science, vol. 6, pp. 344-352, May 1976.

31. J. Wang, The effect of microcracking upon the poisson's ratio for brittle materials, Journal of Material Science, 19 (1984) 809-814.

32. N. Chawla, B.V. Patel, M. Koopman, K.K. Chawla, R. Saha, B.R. Patterson, E.R. Fuller, S.A. Langer, Microstructure-based simulation of thermo-mechanical behavior of composite materials by objected-oriented finite element analysis, Materials Characterization 49 (2003) 395-407.

33. S. Rawal, Metal-Matrix Composites for Space Applications, MMCs for Space, JOM, April 2001.

34. J. Dubský, H.J. Prask, J. Matějíček, T. Gnäupel-Herold, Stresses in plasma-sprayed Cr2O3 coating by neutron diffraction, Applied Physics A (2002).

35. Materials Deposition, Cold Spray, Department of Defense Manufacturing Process Standard, 4 August 2008.

36. C. Borchers, F. Gärtner, and T. Stoltenhoff, H. Assadi, H. Kreya, Microstructural and macroscopic properties of cold sprayed copper coatings, Journal of Applied Physics, Volume 93, Number 12, 15 June 2003.

37. M. P. Planche, H. Liao, C. Coddet, Relationships between in-flight particle characteristics and coating microstructure with a twin arc spray process and different working conditions, 22 April 2004.

38. Denis Bémer, Roland Régnier, Isabelle Subra, Benjamin Sutter, Marie T. Lecler and Yves Morele, Ultrafine Particles Emitted by Flame and Electric Arc Guns for Thermal Spraying of Metals, Annals of Occupational Hygiene. 54 (6): 607-614 (2010).
39. J.N. DuPONT, Soldification of an Alloy 625 Weld Overlay, Metallurgical and Materials Transactions A, 3612-Volume 27A, November 1996.
40. Karl Ulrich Kainer, Basic of Metal Matrix Composites, DOI: 10.1002/3527608117.ch1, 6 June 2006.
41. T. W. Clyne, P. J. Withers, An Introduction to Metal Matrix Composites, Cambridge University Press, Cambridge (1993).
42. M. Bashirzadeh, F. Azarmi, C.P. Leither, G. Karami, Investigation on relationship between mechanical properties and microstructural characteristics of metal matrix composites fabricated by cold spraying technique, 2013.
43. T. S. Srivatsan, M. Al-Hajir, The fatigue and final fracture behavior of SiC particle reinforced 7034 aluminum matrix composites, Composites Part B. 33 (2002) 391-404.
44. F. L. Matthews, R. D. Rawlings, Composite Materials Engineering and Science, first ed., Chapman and Hall, Florida, 1993.
45. C.C. Brendt, W. J. Lenling, Handbook of Thermal Spray Technology, in: J.R. Davis (Ed.), Cold Spray Process, ASM International., Ohio, 2004, pp. 77-84.
46. H. L. Elselstein and D. J. Tillack, The Invention and Definition of Alloy 625, Inco Alloys International, Inc, 1991.
47. J.M. Torralba, C.E. da Costa, F. Velasco, P/M aluminum matrix composites: an overview, Journal of Materials Processing Technology, 133 (2003) 203–206.

48. M. Eizadjou, A. Kazemi Talachi, H. Danesh Manesh, H. Shakur Shahabi, K. Janghorban, Investigation of structure and mechanical properties of multi-layered Al/Cucomposite produced by accumulative roll bonding (ARB) process, Composites Science and Technology 68 (2008) 2003–2009.
49. Betteridge, W., & Shaw, S. (1987). Development of Superalloys. Materials Science and Technology, Volume 3, Number 9, 682-694.
50. Chester T. Sims, N. S. (1987). Superalloys II. New York: John Wiley & Sons.
51. Reed, R. C. (2006). The Superalloys: Fundamentals and Applications. New York: Cambridge University Press.
52. Roger Reed, Physical Metallurgy and Microstructure of Superalloys, Materials Technology, University of Birmingham (Feb 2007).
53. Tresa M. Pollock & S. Tin, Nickel-Based Superalloys for Advanced Turbine Engines: Chemistry, Microstructure, and Properties, Journal of Propulsion and Power, Vol. 22, No. 2, March-April 2006.
54. F. Azarmi and C. P. Leither, Microstructural Formation During Wire Arc Spraying of Alloy 625 on Wrought Alloy 625 Substrate, A Metallurgical and Materials Transactions, 31 July 2012.
55. ASTM International, "Standard Test Method for Tension Testing of Metallic Materials [Metric]" Designation: E 8M-04, Annual Book of ASTM Standards, vol. 03.01, 1997.
56. M.V. Nazarov, T.A. Nazarova, S.N. Dub, G.K. Banini, Nanoindentation, MIcrohardness, and Cathodoluminescense of MgO Crystals, Moldavian Journal of the Physical Sciences, Vol. 2, 2003.

57. W.C. Oliver, G. M. (1992). An improved technique for determining hardness and elastic modulus using load and displacement sensing indentation exerpiments. Journal of Materials Research, 1564-1583.

58. ASTM International. Standard Test Method for Impulse Excitation: E 1876–99, Annual Book of ASTM Standards, Vol 14.02, 2007.

59. I.L. Lim, I.W. Johnston, S.K. Choi, J.N. Boland, Fracture testing of a soft rock with semi-circular specimens under three-point bending test. International Journal of Rock Mechanics and Mining Sciences & Geomechanics, June 1994.

60. ASTM International. “Standard Test Methods for Flexural Properties of Unreinforced and Reinforced Plastics and Electrical Insulating Materials”, April 1 2001.

61. D. P. Hasselman. J. Am Ceram. Soc. 45 (1962) 452-453.

62. Torralba, J. M., C. E. Costa, and F. Velasco. "P/M Aluminum Matrix Composites: An Overview." Materials Processing Technology 133 (2003): 203-06.

63. Ghomashchi, M. R., and A. Vikhrov. "Squeeze Casting: An Overview." Materials Processing Technology 101 (2000): 1-9.

64. S. A. Langer, E. R. Fuller, JR, and W. Craig Carter, OOF: An Image-Based Finite-Element Analysis of Material Microstructures, Mater. Sci. 1 (2001) 15-23.

65. S. Deshpande, A. Kulkarni, S. Sampath, H. Herman, Application of Image Analysis for Characterization of Porosity in Thermal Spray Coatings and Correlation with Small Angle Neutron Scattering, Surf. Coat. Technol.187 (2004) 6– 16.

66. F. L. Matthews, R. D. Rawlings, Composite Materials Engineering and Science, first ed., Chapman and Hall, Florida, 1993.